nature immunology

RESOURCE

https://doi.org/10.1038/s41590-021-00931-3

The multiple myeloma microenvironment is defined by an inflammatory stromal cell landscape

Madelon M. E. de Jong[1], Zoltán Kellermayer[1], Natalie Papazian[1], Sabrin Tahri[1], Davine Hofste op Bruinink[1], Remco Hoogenboezem[1], Mathijs A. Sanders[1], Pieter C. van de Woestijne[2], P. Koen Bos[3], Cyrus Khandanpour[4], Jessica Vermeulen[5], Philippe Moreau[6], Mark van Duin[1], Annemiek Broijl[1], Pieter Sonneveld[1]✉ and Tom Cupedo[1]✉

Progression and persistence of malignancies are influenced by the local tumor microenvironment, and future eradication of currently incurable tumors will, in part, hinge on our understanding of malignant cell biology in the context of their nourishing surroundings. Here, we generated paired single-cell transcriptomic datasets of tumor cells and the bone marrow immune and stromal microenvironment in multiple myeloma. These analyses identified myeloma-specific inflammatory mesenchymal stromal cells, which spatially colocalized with tumor cells and immune cells and transcribed genes involved in tumor survival and immune modulation. Inflammatory stromal cell signatures were driven by stimulation with proinflammatory cytokines, and analyses of immune cell subsets suggested interferon-responsive effector T cell and CD8$^+$ stem cell memory T cell populations as potential sources of stromal cell–activating cytokines. Tracking stromal inflammation in individuals over time revealed that successful antitumor induction therapy is unable to revert bone marrow inflammation, predicting a role for mesenchymal stromal cells in disease persistence.

Cancer development and progression are accompanied by alterations in the local tissue microenvironment[1], which encompasses both hematopoietic and non-hematopoietic cells as well as non-cellular elements, such as extracellular matrix (ECM) and soluble factors[2,3]. In multiple myeloma (MM), a hematological malignancy characterized by the accumulation of malignant plasma cells in the bone marrow, interactions between myeloma cells and their environment are considered critical for disease pathobiology[2]. Mesenchymal stromal cells (MSCs) are an integral part of the non-hematopoietic bone marrow microenvironment,[4,5] and MSC-derived cytokines, such as interleukin-6 (IL-6), have been established as essential for MM tumorigenesis and progression[6,7]. Nonetheless, the identity of the MSCs associated with MM in vivo and whether MSCs also direct immune alterations within MM bone marrow remain undefined. Changes in bone marrow immune cell populations are already present during MM precursor stages[8,9] and include a selective reduction in cytotoxic memory T cells important for sustained antitumor immunity[10,11] and an increase in several immune-suppressive cell populations, involving regulatory T cells (T_{reg}) and myeloid-derived suppressor cells (MDSCs)[12,13].

Treatment of MM has improved significantly by the introduction of immune therapies, including immunomodulatory imide drugs (IMiDs), proteasome inhibitors and antibodies targeting tumor- and immune cell-expressed proteins, such as CD38 (refs. [14,15]). This notwithstanding, treatment invariably fails to fully eradicate malignant plasma cells, and most individuals, even those with excellent therapy response, eventually experience disease relapse. MM therefore remains an incurable disease[16]. Targeting MM cells in combination with the tumor-supportive bone marrow microenvironment holds the potential of increasing therapy efficacy; yet, it is hampered by an incomplete definition of this microenvironment.

In this study, we generated paired single-cell RNA-sequencing datasets of the non-hematopoietic microenvironment, CD38$^+$ and CD38$^-$ immune microenvironments together with tumor cells from 13 newly diagnosed individuals with MM and 7 non-cancer control individuals undergoing cardiac surgery or hip-replacement surgery, creating a unique resource allowing for in-depth analyses of stromal–immune–tumor interactions within the bone marrow microenvironment. This led to the identification of inflammatory MSCs (iMSCs) specific for MM bone marrow. iMSC development was likely the result of activation caused by inflammatory mediators activating NF-κB signaling, such as tumor necrosis factor (TNF) and IL-1β. Within the MM-containing bone marrow, TNF was transcribed by CD8$^+$ stem cell memory T (T_{scm}) cells and interferon (IFN)-responsive effector T cells, which are increased in MM compared to controls, suggesting the presence of immune cell-mediated stromal inflammation. Using ligand–receptor interaction analyses, we identified a putative role for iMSCs in the regulation of cycling plasma cells and in the modulation of myeloid cell function. Finally, by tracking iMSC signatures and inflammatory cytokines over time in individuals undergoing first-line treatment, we show that bone marrow inflammation is not reverted by successful antitumor therapy, suggesting a role for iMSCs and bone marrow inflammation in disease persistence or relapse.

Results

Composition of the human non-hematopoietic bone marrow niche. To define the human non-hematopoietic bone marrow microenvironment, we generated a single-cell transcriptomic overview of the non-hematopoietic mononuclear cell fraction from viably frozen bone marrow aspirates from 13 newly diagnosed individuals with myeloma and 7 age-matched control patients.

[1]Department of Hematology, Erasmus MC Cancer Institute, Erasmus Medical Center, Rotterdam, the Netherlands. [2]Department of Cardiothoracic Surgery, Erasmus Medical Center, Rotterdam, the Netherlands. [3]Department of Orthopedic Surgery, Erasmus Medical Center, Rotterdam, the Netherlands. [4]Medical Department A, University Hospital Münster, Münster, Germany. [5]Janssen Research & Development LLC, Leiden, the Netherlands. [6]Nantes University Hospital Hotel-Dieu, Nantes, France. ✉e-mail: p.sonneveld@erasmusmc.nl; t.cupedo@erasmusmc.nl

Characteristics of individuals with myeloma and control individuals are described in Supplementary Tables 1–3. Purification was based on flow cytometric exclusion of hematopoietic cells (CD45), erythroid lineage cells (CD235, CD71) and plasma cells (CD38), and the presence of non-hematopoietic cells was verified by the expression of CD271, CD105, CD31 and CD34 (for gating strategy, see Extended Data Fig. 1a). On average, the non-hematopoietic bone marrow niche comprised 0.002% of total aspirated cells (Extended Data Fig. 2a). Sequencing generated single-cell transcriptomes of 19,983 cells from MM bone marrow and 7,038 cells from control bone marrow, which were integrated into a single dataset (Fig. 1a). We identified five closely related mesenchymal stromal cell clusters (MSC1–MSC5), as defined by the transcription of *LEPR* and *CXCL12* (Fig. 1b). In contrast to the non-hematopoietic niche in mice[4], no clear distinction between MSCs and fibroblasts was apparent, as clusters MSC1–MSC5 also transcribed fibroblast-associated markers *FN1* and *DCN* (Extended Data Fig. 2b) and various types of collagens (Fig. 1b and Extended Data Fig. 2c). Moreover, genes whose mouse orthologs denote distinct mouse MSC subsets, such as *CXCL12*, *LEPR*, *PDGFRA*, *PDGFRB* and *ACTA2*, were equally transcribed between mesenchymal clusters (Fig. 1b and Extended Data Fig. 2d). A single cluster of endothelial cells was defined by transcription of *CDH5*, *THBD* and *CD36* (cluster EC, Fig. 1b and Extended Data Fig. 2e). Cluster SEC (*SELP*$^+$ cells) was defined by specific transcription of *SELP* (encoding P-selectin) (Fig. 1b), a feature of activated endothelial cells[17]; yet, cells in this cluster did not transcribe detectable *CDH5* or increased levels of *CD36* (Extended Data Fig. 2e) nor genes associated with MSC transcriptomes, such as collagens, *LEPR* or *CXCL12* (Fig. 1b and Extended Data Fig. 2c). The genes driving clustering of these cells are listed in Supplementary Table 4. Due to the bias for marrow cells introduced by sample aspiration rather than biopsy, only a single small cluster of osteolineage cells specifically transcribing *RUNX2* and *SP7* (cluster OLC, Fig. 1b and Extended Data Fig. 2f) was present. In sum, the data presented here provide a comprehensive single-cell transcriptomic database of the human non-hematopoietic bone marrow microenvironment.

Identification of myeloma-specific iMSCs. To identify MM-specific MSC alterations, uniform manifold approximation and projection (UMAP) renderings were split into individuals with MM and non-cancer control individuals. This identified two MSC clusters (MSC1 and MSC2) that were strongly enriched in MM bone marrow (Fig. 1c and Extended Data Fig. 2g,h). Ranked gene set enrichment analysis (GSEA) comparing clusters MSC1 and MSC2 to clusters MSC3, MSC4 and MSC5 showed significant enrichment for the inflammation-related pathway 'TNFα signaling via NFκB' (Fig. 1d). Genes driving this pathway were mostly inflammatory genes with increased transcription in clusters MSC1 and MSC2, including MM cell survival factors *IL6* and *LIF*[18,19], chemokines involved in immune cell migration (*CXCL2*, *CXCL3*, *CXCL5*, *CXCL8* and *CCL2* (refs. [20,21])), modulator of the T cell response *PTGS2* (ref. [22]), cytokine receptor *IL1RL1* and *CD44*, a receptor protein involved in cellular interactions that is expressed by solid tumor-associated fibroblasts[23,24] (Fig. 1e). All of these transcripts were either absent or detected at lower levels in both the non-cancer control dataset and in the non-inflammatory remainder of the MSCs in myeloma (MSC3–MSC5) (Fig. 1e). From here onwards, we will refer to the myeloma-specific clusters MSC1 and MSC2 as iMSCs. Supplementary Tables 5 and 6 and Extended Data Fig. 2k detail all differentially expressed genes and altered pathways between clusters MSC1/MSC2 and the remainder of the MSCs, while Supplementary Table 7 lists the differentially expressed genes between clusters MSC1 and MSC2. The iMSC clusters were detected in all individuals with MM that were analyzed, irrespective of the genetic makeup of the tumor, and were virtually absent from all non-cancer control individuals (Fig. 1f,h and Extended Data Fig. 2g,h). Moreover, iMSCs were also detected in a fresh sample that was immediately sequenced after aspiration (Extended Data Fig. 3a,b). Differential analyses of individuals with translocations and individuals with a hyperdiploid genome suggested minor differences in the MSC1/MSC2 ratio (Fig. 1g,h). However, the high degree of variation (Extended Data Fig. 2h) and the limited number of individuals in each respective group warrants caution in interpreting any differences and did not allow for robust correlations of iMSC abundance with any clinical parameters, such as the revised international staging system (R-ISS) stage or tumor load (Extended Data Fig. 2i,j). The inflammatory bone marrow environment suggested by iMSC presence was confirmed by elevated protein levels of IL-6, CXCL8 and CCL2 in the bone marrow plasma of individuals with myeloma compared to age-matched non-cancer control individuals (Fig. 1i). No correlation between levels of inflammatory cytokines and iMSC percentages was apparent (Extended Data Fig. 3c). Clusters containing endothelial cells and *SELP*$^+$ cells were also increased in individuals with MM compared to non-cancer control individuals (Fig. 1h and Extended Data Fig. 2g); yet, the relative scarcity of the cells in these populations precluded detailed analyses. Given the potential niche function of endothelial cells in MM[25], these clusters are of interest for further exploration. In summary, our findings reveal MM-specific bone marrow inflammation and the presence of iMSCs that transcribe myeloma cell survival factors and inflammatory genes implicated in immune cell recruitment and immune modulation.

In situ localization of myeloma-specific iMSCs. A prerequisite for a role of iMSCs in MM pathobiology would be their colocalization with tumor cells or immune cells in situ. To analyze the spatial distribution of iMSCs, fluorescent immunohistochemistry was performed on iliac crest bone marrow biopsies of newly diagnosed individuals with MM and non-cancer control individuals. *CD44* transcription was enriched in the iMSC clusters and was also enriched at the protein level, as determined by flow cytometry on CD271$^+$ MSCs in newly diagnosed individuals with MM versus in non-cancer control individuals (Fig. 2a and Extended Data Fig. 4a). Therefore, we used CD44 in combination with the pan-MSC marker CXCL12 to identify MSCs in situ. Cells with mesenchymal morphology expressing both CXCL12 and CD44 were readily identified scattered throughout the MM bone marrow (Fig. 2b, white arrows). In non-myeloma bone marrow, CXCL12$^+$CD44$^+$ mesenchymal-like cells were virtually absent, and only an occasional cell could be identified (Fig. 2c). CXCL12$^+$CD44$^+$ iMSCs were always interacting with CD138$^+$ MM cells (Fig. 2b) and/or CD3$^+$ T cells (Fig. 2d). This notwithstanding, there was also a substantial fraction of MM cells as well as T cells that did not interact with iMSCs. The MM bone marrow also specifically contained adipocytes expressing CD44 (Fig. 2b), a known marker of adipocyte activation[26]. These data show that iMSCs are in the anatomically correct position to influence both MM cells and T cells.

iMSC appearance is driven by cellular activation. In MM, clusters MSC1–MSC5 represented a largely homogenous group of *CXCL12*$^+$*LEPR*$^+$ marrow mesenchymal cells with comparable transcription levels of various canonical MSC markers as well as most ECM-encoding genes (Fig. 1b and Extended Data Fig. 2b,c). Because GSEA had indicated NF-κB activation as a possible mechanistic driver of inflammatory gene expression (Fig. 1d), we hypothesized that myeloma-specific alterations were the result of cell activation rather than lineage differentiation. Text mining and analysis of available coexpression databases using STRING[27] indicated that TNF and IL-1β signaling were associated with all of the inflammatory genes detected in clusters MSC1 and MSC2 (Fig. 3a). *TNFRSF1A* and *TNFRSF1B* (encoding TNF-RI and TNF-RII) (Fig. 3b) as well as *IL1R* (encoding the IL-1 receptor)

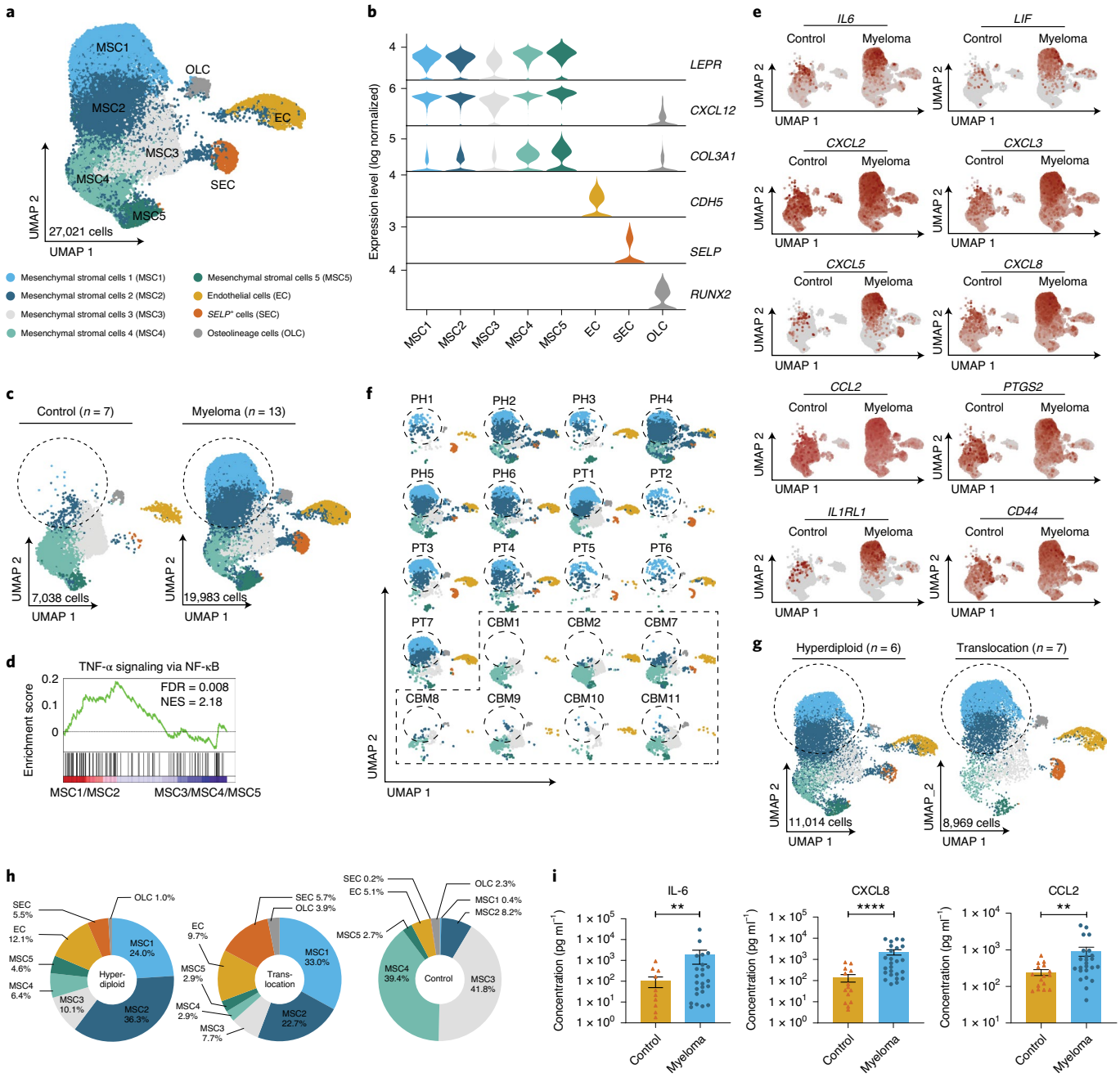

Fig. 1 | Identification of myeloma-specific inflammatory MSCs. a, UMAP of the combined dataset of 19,983 cells from 13 individuals with myeloma and 7,038 cells from 7 non-cancer control individuals showing eight clusters identified by integrated analysis. Colors represent clusters. **b**, Violin plots of marker gene transcription in the eight clusters. **c**, Original UMAP split into control (non-cancer) and myeloma datasets. **d**, GSEA enrichment plot for the gene set 'TNFα signaling via NFκB' in clusters MSC1 and MSC2 as compared to clusters MSC3, MSC4 and MSC5; FDR, false discovery rate; NES, normalized enrichment score. **e**, Transcription of differentially expressed genes in control or myeloma non-hematopoietic bone marrow. **f**, Original UMAP split by individual. CBM, control bone marrow; PH, individual with a hyperdiploid tumor; PT, individual with a tumor harboring translocations. **g**, Original UMAP split by genetic background of tumor. **h**, Circle diagrams depicting cluster fractions of totals in individuals with tumors bearing hyperdiploidies ($n = 6$) or translocations ($n = 7$) or in non-cancer control individuals (control) ($n = 7$). **i**, Bar graphs depicting IL-6, CXCL8 and CCL2 protein levels in the bone marrow plasma of individuals with myeloma ($n = 25$) and non-cancer control individuals ($n = 18$). Data are presented as mean ± s.e.m. Significance was calculated using the Mann–Whitney *U* test (two-tailed); $^{**}P \leq 0.01$ and $^{****}P \leq 0.0001$.

and *IL1RAP* (encoding IL-1 receptor accessory protein) (Fig. 3c) were transcribed by all MSC clusters, implicating TNF and IL-1β as possible activators of myeloma iMSCs. IL-1β protein levels were increased in the bone marrow plasma of individuals with MM compared to in non-cancer control individuals (Fig. 3d), while plasma TNF levels were below the levels required for reliable detection. To directly address whether cytokine activation could induce an iMSC-like transcriptome, we stimulated ex vivo-expanded human bone marrow-derived MSCs in vitro. Overnight stimulation of primary MSCs from individuals with MM with either TNF or IL-1β led

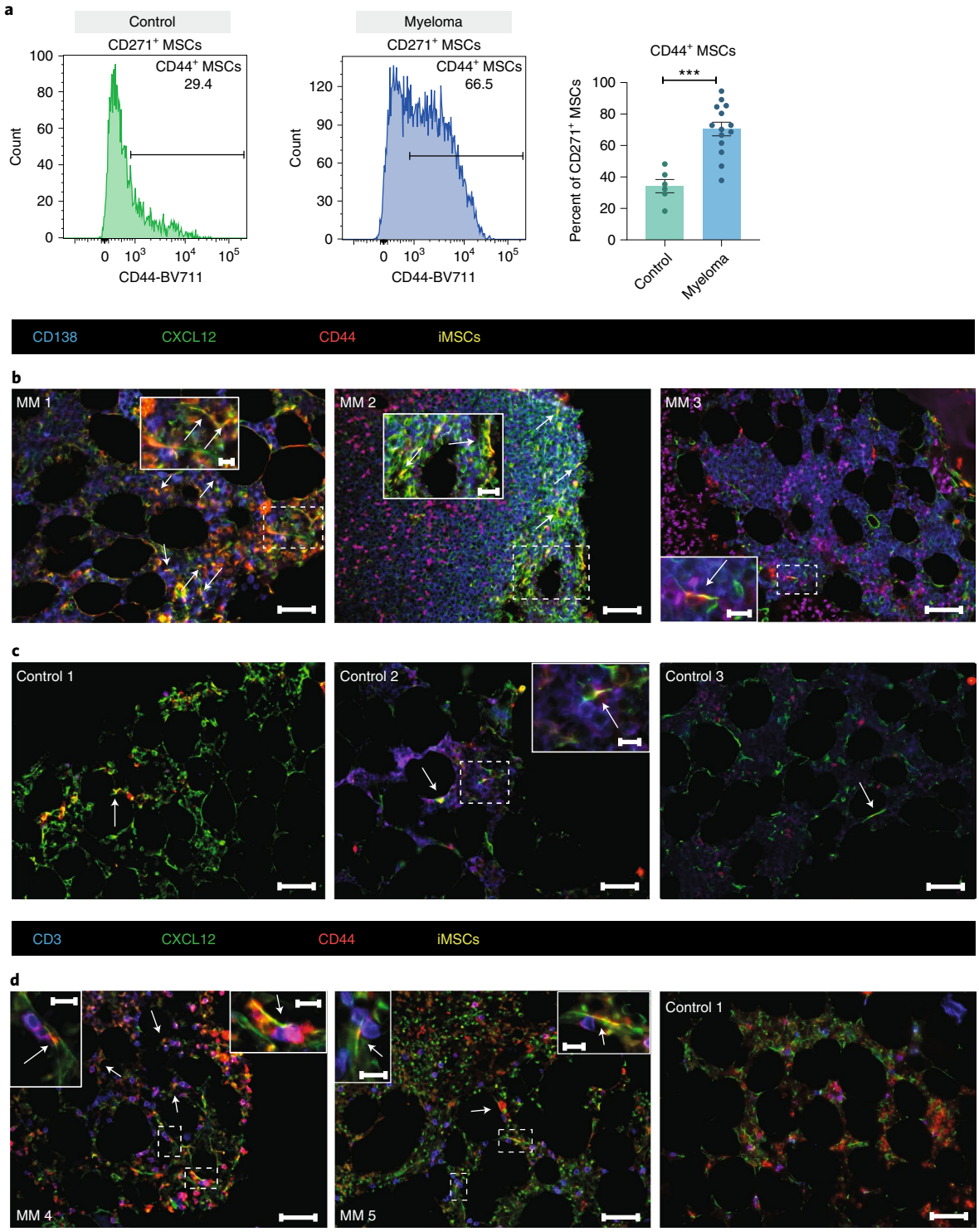

Fig. 2 | Distinct localization of CD44⁺ iMSCs in bone marrow. a, Flow cytometric analyses of CD44 protein expression on CD271⁺ MSCs in individuals with myeloma ($n = 14$) and non-cancer control individuals (control; $n = 6$). Data are presented as mean ± s.e.m. Significance was calculated using the Mann–Whitney *U* test (two-tailed); $^{***}P \leq 0.001$. **b**, Immunofluorescence staining of bone marrow biopsies from newly diagnosed individuals with MM depicting plasma cells (CD138, blue), non-inflammatory MSCs (CXCL12, green) and iMSCs (CXCL12/CD44, orange color and white arrows); scale bars, 50 µm (overviews) and 10 µm (insets). Representative images are depicted; total *n* of tested individuals = 20 in four individual experiments. **c**, Immunofluorescence staining of bone marrow biopsies from non-cancer control individuals depicting plasma cells (CD138, blue), non-inflammatory MSCs (CXCL12, green) and iMSCs (CXCL12/CD44, orange color and white arrows); scale bars, 50 µm (overviews) and 10 µm (inset). Representative images are depicted; total *n* of tested individuals = 5 in four individual experiments. **d**, Immunofluorescence staining of bone marrow biopsies from individuals with myeloma and non-cancer control individuals depicting T cells (CD3, blue), non-inflammatory MSCs (CXCL12, green) and iMSCs (CXCL12/CD44, orange color and white arrows); scale bars, 50 µm (overviews) and 10 µm (insets). Representative images are depicted; total *n* of tested individuals with myeloma = 10 and tested non-cancer control individuals = 2 in two independent experiments.

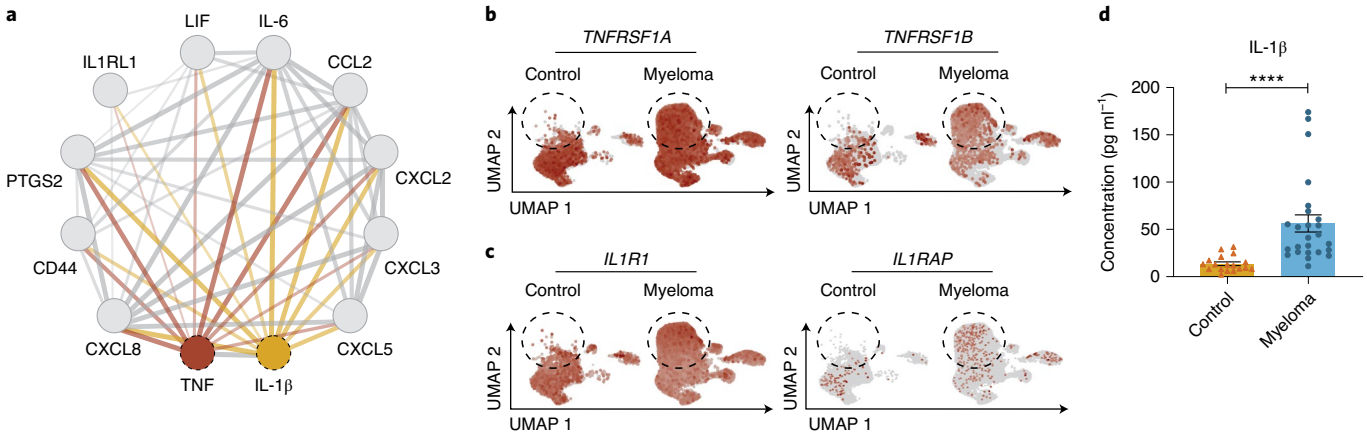

Fig. 3 | Potential activators of iMSCs. a, STRING network analysis of iMSC-expressed immune-related proteins in relation to TNF and IL-1β. Line thickness indicates confidence. **b**, Transcription of *TNFRSF1A* and *TNFRSF1B* in non-cancer control or myeloma non-hematopoietic bone marrow. **c**, Transcription of *IL1R1* and *IL1RAP* in non-cancer control or myeloma non-hematopoietic bone marrow. **d**, Bar graph depicting IL-1β protein levels in bone marrow plasma from individuals with myeloma and from non-cancer control individuals. Data are presented as mean ± s.e.m. Significance was calculated using the Mann–Whitney *U* test (two-tailed); $^{****}P \leq 0.0001$.

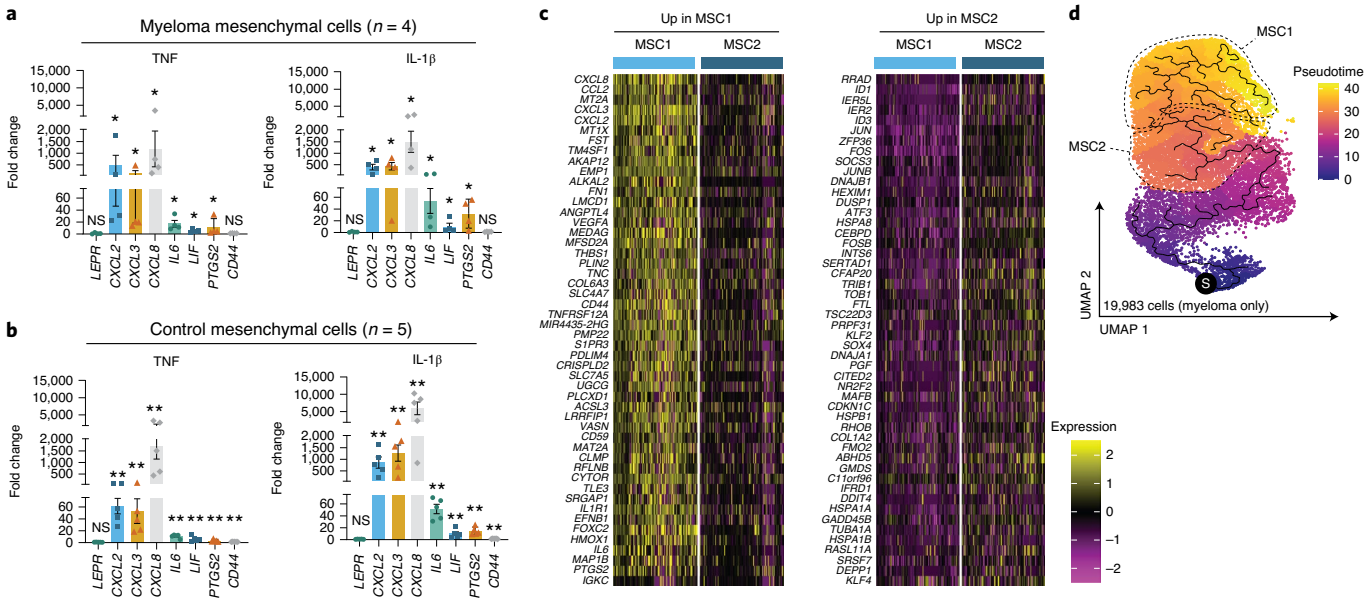

Fig. 4 | Activation recapitulates stromal inflammation. a, Transcription of inflammatory genes as determined by qPCR after stimulation of in vitro-expanded myeloma MSCs with recombinant human (rh) TNF or rhIL-1β. Fold change is proportionate to transcription under unstimulated conditions. Results are from four stromal cultures derived from individuals with MM. **b**, Transcription of inflammatory genes as determined by qPCR after stimulation of in vitro-expanded non-myeloma control MSCs with rhTNF or rhIL-1β. Fold change is proportionate to transcription under unstimulated conditions. Results are from five stromal cultures derived from non-cancer control individuals. **c**, Heat map of the top 50 differentially expressed genes that were upregulated in MSC1 as compared to MSC2 (left) or upregulated in MSC2 as compared to MSC1 (right). **d**, Monocle 3 pseudotime analysis of MSCs in individuals with myeloma. 'S' represents an arbitrarily selected starting point of trajectory calculations. The data in **a** and **b** are presented as mean ± s.e.m. Significance was calculated using the Mann–Whitney *U* test (two-tailed); NS, $P > 0.05$; $^{*}P \leq 0.05$; $^{**}P \leq 0.01$.

to increased transcription of *IL6*, *LIF*, *CXCL2*, *CXCL3*, *CXCL8* and *PTGS2* (Fig. 4a). This response was not restricted to cells from MM bone marrow, as MSCs from non-cancer control individuals also acquired an iMSC-like transcriptome upon stimulation with TNF or IL-1β (Fig. 4b) (see Supplementary Tables 1 and 8 for clinical characteristics of MSC donors). The differentially expressed inflammatory genes that drove clustering of iMSCs were consistently transcribed at higher levels in MSC1 compared to MSC2 (Fig. 4c), suggesting that cluster MSC2 may represent an intermediate state of activation. In agreement, pseudotime analysis predicted that with a pseudo starting point at cluster MSC5, the trajectory of transcriptional changes from non-inflammatory MSCs to MSC1 can only progress via cluster MSC2 (Fig. 4d and Extended Data Fig. 3d). Together, these experiments show that activation of MSCs is sufficient to induce the inflammatory transcriptome associated with MM iMSCs.

Bone marrow immune cell alterations in newly diagnosed MM. Myeloma cells as well as various immune cell subsets are previously reported sources of iMSC-inducing cytokines TNF and IL-1β (ref. [28]). To further dissect niche interactions in MM, lymphocytes, granulocytes, CD14$^+$ myeloid cells and CD138$^+$ plasma cells were purified from fresh bone marrow aspirates from four additional newly diagnosed individuals with myeloma (for gating strategy, see Extended Data Fig. 1b), and transcription of *TNF* and *IL1B* were analyzed by qPCR. Transcription of *TNF* was highest in lymphocytes followed by myeloid cells (Fig. 5a). *IL1B* was mainly transcribed by myeloid cells (Fig. 5a). In contrast to earlier reports[28,29], the plasma cells in this small cohort did not transcribe detectable levels of either of these cytokines. Hypothesizing that iMSC appearance could be linked to local inflammation, we set out to identify specific subsets of lymphoid and myeloid cells capable of activating iMSCs. To this end, single-cell RNA-sequencing datasets were generated from 134,000 sorted CD38$^-$ and 128,000 sorted CD38$^+$ hematopoietic cells from the same 13 newly diagnosed individuals with MM used for non-hematopoietic cell isolation in Fig. 1 as well as from 5 non-cancer control individuals (for gating strategy see Extended Data Fig. 1c, and for participant details see Supplementary Tables 1–3). In light of recent developments in immunotherapies using monoclonal anti-CD38, we opted to sort and analyze CD38$^+$ hematopoietic cells as a separate dataset, thereby increasing the resolution for subsets expressing this clinically relevant surface protein. MM cells were separated from the CD38$^+$ dataset in silico before further analyses, yielding a separate dataset of 32,000 myeloma cells from these 13 individuals.

Combined, the two hematopoietic datasets captured all major bone marrow immune subsets except for polynuclear myeloid cells, which were lost as a result of mononuclear cell isolation and a freeze–thaw cycle during work-up. The CD38$^-$ dataset was enriched for adaptive immune cells (Fig. 5b,c), with a predominance of *CD4*$^+$ T cells, including *SELL*$^+$*CCR7*$^+$ naive helper T cells, *IFNG*$^+$*TBX21*$^+$ type 1 helper (T_H1) cells, *IL4*$^+$ T_H2 cells, *FOXP3*$^+$ T_{reg} cells and *RORC*$^+$ T_H17 cells (Fig. 5b,c and Extended Data Fig. 5a). In individuals with myeloma, there was a trend toward an increased CD4/CD8 ratio (Fig. 5d) and a significant decline of CD38$^-$*FOXP3*$^+$ T_{reg} cells compared to non-cancer control individuals (Fig. 5d). *CD8*$^+$ T cells were comprised of a cluster of *SELL*$^+$*CCR7*$^+$ naive cytotoxic T cells as well as early (*GZMK*$^+$) and late (*GZMB*$^+$) effector T cell clusters (Fig. 5b,c) at a ratio of 1:2 (Fig. 5d), which was similar in control individuals and individuals with myeloma. Interestingly, a cluster containing type I IFN-responsive CD8$^+$ and CD4$^+$ T cells was defined by the expression of *IFIT1*, *IFIT2* and *IFIT3* (Extended Data Fig. 5b) and was expanded in individuals with myeloma compared to control patients (Fig. 5d). The CD38$^-$ dataset also contained one cluster of *NCR1*$^+$ NK cells, three clusters of *MS4A1*$^+$ B cells and a small cluster of *LYZ*$^+$ monocytes (Fig. 5b,c and Extended Data Fig. 5a). Finally, some erythrocyte admixture was present. Dataset composition was conserved among individuals (Extended Data Fig. 3f).

The CD38$^+$ dataset contained five large clusters of *LYZ*$^+$ myeloid cells (Fig. 5e,f), including two clusters of *CD14*$^+$ classical monocytes, one cluster of *CD14*$^+$ monocytes partially coexpressing *FCGR3A* (encoding CD16; Extended Data Fig. 5c), suggestive of intermediate monocytes, a cluster of *ELANE*$^+$*CD14*$^+$ monocytes and a cluster of *FCER1A*$^+$*CD1C*$^+$*CD14*$^+$ monocyte-derived dendritic cells (Fig. 5e,f). The T cells in this dataset were mainly helper T cells (Fig. 5e,f) and were composed of a cluster of naive *CCR7*$^+$*CD4*$^+$ helper T cells, which was reduced in frequency in individuals with myeloma compared to control patients(Fig. 5g), and a cluster of mixed helper T cells, including some *FOXP3*$^+$ T_{reg} cells (Fig. 5e,f). In addition, a cluster of *GZMB*$^+$*CD8B*$^+$ effector T cells and one cluster of *CCR7*$^-$*CXCR3*$^+$*CD27*$^+$*FAS*$^+$*GZMK*$^+$*CD8*$^+$ T_{scm} cells were present (Fig. 5e,f). Previous studies reported a decline in frequency of the T_{scm} population in MM bone marrow compared to bone marrow from precursor stages monoclonal gammopathy of undetermined significance (MGUS) and/or smoldering MM (SMM)[10,11]. Here, we found CD8 T_{scm} to be expanded in MM bone marrow compared to in the bone marrow of non-cancer control patients, both by single-cell RNA sequencing (Fig. 5g) and by flow cytometry (Fig. 5h), suggesting a progression-dependent dynamic in the frequency of these cells. In line with existing literature on CD38 expression on NK cells[30], three *NRC1*$^+$*CD3D*$^-$ clusters were present: one cluster of *GZMK*$^+$*CX3CR1*$^-$CD56^{bright} NK cells[31] and two clusters of *GZMB*$^+$*CX3CR1*$^+$CD56^{dim} NK cells (Fig. 5e,f and Extended Data Fig. 5c–e). Previously, increased NK cell frequency had been associated with significant enrichment for GZMK$^+$CX3CR1$^-$CD56^{bright} NK cells[9], and, in line with those data, we observed a significant increase in *GZMK*$^+$*CX3CR1*$^-$CD56^{bright} NK cells in MM bone marrow by single-cell RNA sequencing (Fig. 5g) as well as a significant increase in total CD56^{bright} NK cells (Fig. 5h) and CD56^{bright}CD27$^+$ NK cells (Fig. 5h and Extended Data Fig. 5c–e) by flow cytometry. B cell clusters reflected various developmental stages, including *VPREB1*$^+$*MKI67*$^+$ pre-B cells and *MS4A1*$^+$ mature B cells (Fig. 5e,f). The composition of the dataset was conserved between individuals (Extended Data Fig. 5g).

The dataset containing myeloma plasma cells consisted of six clusters with homogeneous transcription of canonical myeloma cell markers, including *SDC1* and *CXCR4* (Extended Data Fig. 6a,b). Cluster 1 consisted of cycling *MKI67*$^+$ plasma cells (Extended Data Fig. 6a,b). Cluster 4 contained *SDC1*$^+$ mature B cells, which coexpressed *MS4A1* but not *VPREB1* (Extended Data Fig. 6b). Composition of the dataset was conserved between individuals (Extended Data Fig. 6c). In sum, the myeloma bone marrow is characterized by the expansion of IFN-responsive T cells, CD8$^+$ T_{scm} cells and *GZMK*$^+$*CX3CR1*$^-$CD56^{bright} NK cells, while the distribution of many other T cell, B cell and mononuclear myeloid cell populations was unaltered, suggesting specificity in the myeloma-induced adjustments to the bone marrow immune microenvironment.

Immune cell subsets with the capacity to activate MSCs. To identify immune cell subclusters in MM bone marrow with the ability to activate MSCs, we analyzed the transcription of *TNF* and *IL1B*, the cytokines capable of inducing an iMSC-like transcriptome in vitro (Fig. 4a,b). In the *CD38*$^+$*SDC1*$^+$ myeloma cell dataset, neither

Fig. 5 | The myeloma immune microenvironment at single-cell resolution. a, Transcription of *TNF* and *IL1B* as determined by qPCR on major immune cell subsets in the myeloma bone marrow (lymphocytes, $n=5$; granulocytes, $n=6$; myeloid cells, $n=4$; plasma cells, $n=5$). **b**, UMAPs of CD38$^-$ hematopoietic cells from 13 individuals with myeloma (98,246 cells) and 5 non-cancer control individuals (36,233 cells) showing 19 clusters identified by integrated analysis. **c**, Transcription of marker genes in the CD38$^-$ dataset. **d**, Bar graphs depicting quantification of CD38$^-$ cell populations. Data points represent individuals (myeloma, $n=13$; control, $n=7$). **e**, UMAPs of CD38$^+$ hematopoietic cells from 13 individuals with myeloma (60,222 cells) and 5 individuals without myeloma (36,247 cells) showing 18 clusters identified by integrated analysis. **f**, Transcription of marker genes in the CD38$^+$ dataset. **g**, Bar graphs depicting quantifications of CD38$^+$ cell populations. Data points represent individuals (myeloma, $n=13$; control, $n=7$). **h**, Bar graphs depicting quantifications of CD38$^+$CD3$^+$CD8$^+$CD45RA$^+$CD27$^+$FAS$^+$ T_{scm} cells, CD38$^+$CD3$^-$CD56^{bright} natural killer (NK) cells and CD38$^+$CD3$^-$CD56^{bright}CD27$^+$ NK cells as determined by flow cytometry. See Supplementary Table 10 for participant characteristics. Data points represent individuals (myeloma, $n=15$; control, $n=5$). The data in **a**,**d**,**g** and **h** are presented as mean ± s.e.m. Significance was calculated using the Mann–Whitney *U* test (two-tailed). NS, $P>0.05$; $^*P\leq0.05$; $^{**}P\leq0.01$; $^{***}P\leq0.001$.

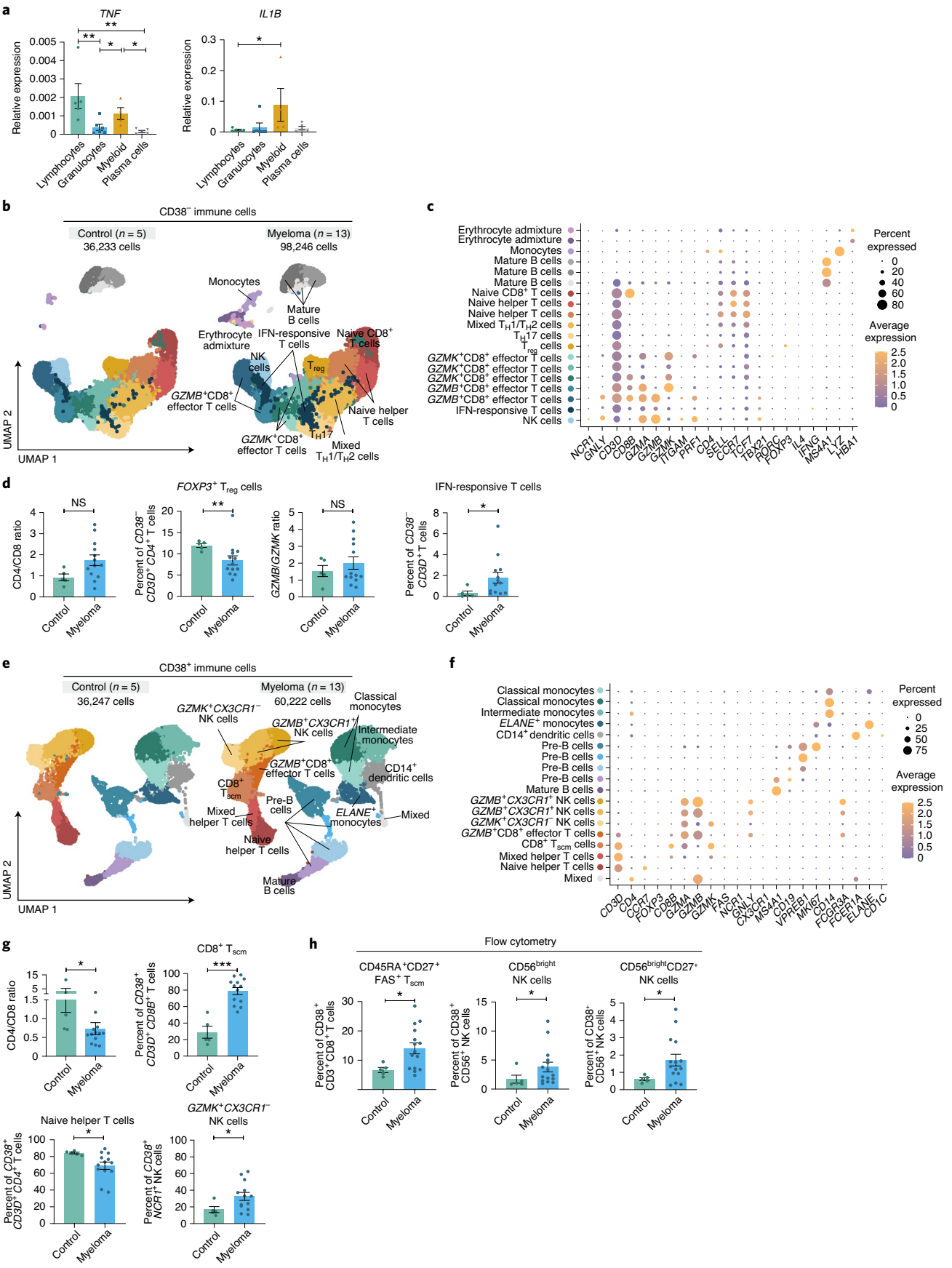
a
TNF
IL1B
Relative expression
Lymphocytes
Granulocytes
Myeloid
Plasma cells
b
CD38⁻ immune cells
Control (n = 5)
36,233 cells
Myeloma (n = 13)
98,246 cells
Monocytes
Mature B cells
Erythrocyte admixture
IFN-responsive T cells
Naive CD8⁺ T cells
NK cells
Treg
GZMB⁺CD8⁺ effector T cells
Naive helper T cells
GZMK⁺ effector T cells
TH17
Mixed TH1/TH2 cells
UMAP 1
UMAP 2
c
Erythrocyte admixture
Monocytes
Mature B cells
Naive CD8⁺ T cells
Naive helper T cells
Mixed TH1/TH2 cells
TH17 cells
Treg cells
GZMK⁺CD8⁺ effector T cells
GZMB⁺CD8⁺ effector T cells
IFN-responsive T cells
NK cells
NCR1 GNLY CD3D CD8B GZMA GZMB GZMK ITGAM PRF1 CD4 SELL CCR7 TCF7 TBX21 RORC FOXP3 IL4 IFNG MS4A1 LYZ HBA1
Percent expressed
Average expression
d
FOXP3⁺ Treg cells
IFN-responsive T cells
CD4/CD8 ratio
Percent of CD38⁻ CD3D⁺ CD4⁺ T cells
GZMB/GZMK ratio
Percent of CD38⁻ CD3D⁺ T cells
NS
Control
Myeloma
e
CD38⁺ immune cells
Control (n = 5)
36,247 cells
Myeloma (n = 13)
60,222 cells
GZMK⁺CX3CR1⁻ NK cells
GZMB⁺CX3CR1⁺ NK cells
Classical monocytes
Intermediate monocytes
GZMB⁺CD8⁺ effector T cells
CD14⁺ dendritic cells
CD8⁺ Tscm
Pre-B cells
Mixed helper T cells
ELANE⁺ monocytes
Mixed
Naive helper T cells
Mature B cells
UMAP 1
UMAP 2
f
Classical monocytes
Intermediate monocytes
ELANE⁺ monocytes
CD14⁺ dendritic cells
Pre-B cells
Mature B cells
GZMB⁺CX3CR1⁺ NK cells
GZMK⁺CX3CR1⁻ NK cells
GZMB⁺CD8⁺ effector T cells
CD8⁺ Tscm cells
Mixed helper T cells
Naive helper T cells
Mixed
CD3D CD4 CCR7 FOXP3 CD8B GZMA GZMB GZMK FAS NCR1 GNLY CX3CR1 MS4A1 CD19 VPREB1 MKI67 CD14 FCGR3A FCER1A ELANE CD1C
Percent expressed
Average expression
g
CD4/CD8 ratio
CD8⁺ Tscm
Percent of CD38⁺ CD3D⁺ CD8B⁺ T cells
Naive helper T cells
Percent of CD38⁺ CD3D⁺ CD4⁺ T cells
GZMK⁺CX3CR1⁻ NK cells
Percent of CD38⁺ NCR1⁺ NK cells
h
Flow cytometry
CD45RA⁺CD27⁺ FAS⁺ Tscm
CD56bright NK cells
CD56brightCD27⁺ NK cells
Percent of CD38⁺ CD3⁺ CD8⁺ T cells
Percent of CD38⁺ CD56⁺ NK cells
Control
Myeloma

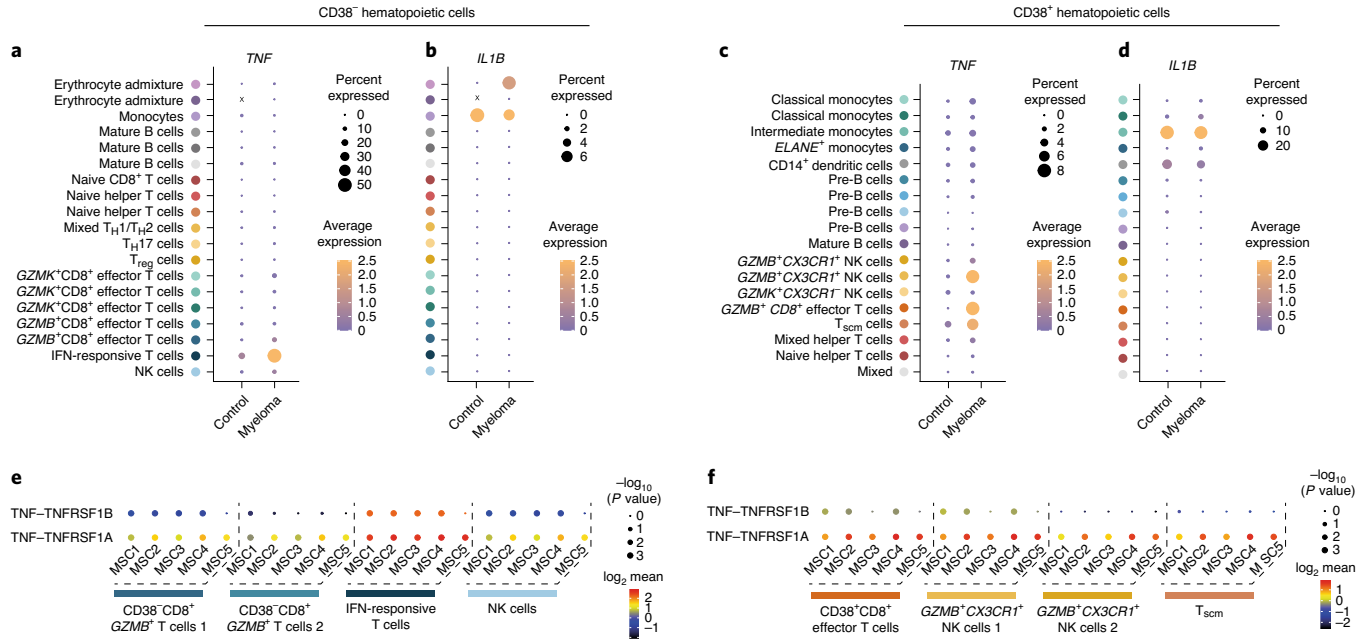

Fig. 6 | Predicted interactions of iMSCs with myeloma cells. Transcription of *TNF* (**a**) and *IL1B* (**b**) in the CD38⁻ dataset. The x marks populations that were absent in the control dataset. Transcription of *TNF* (**c**) and *IL1B* (**d**) in the CD38⁺ dataset. **e**, Predicted TNF–*TNFRSF1A* and TNF–*TNFRSF1B* interactions between MSC clusters and CD38⁻ immune cell clusters. Means and *P* values were calculated using the statistical framework of CellPhoneDB[31]. **f**, Predicted TNF–*TNFRSF1A* and TNF–*TNFRSF1B* interactions between MSC clusters and CD38⁺ immune cell clusters. Means and *P* values were calculated using the statistical framework of CellPhoneDB[31].

TNF nor *IL1B* were transcribed (Extended Data Fig. 6d). In the CD38⁻ dataset, highest levels of *TNF* transcription were found in the IFN-responsive T cell population (Fig. 6a) that was enriched in MM bone marrow (Fig. 5d), with 50% of cells expressing this cytokine. *IL1B* transcription was restricted to myeloid cells, which in this dataset are, in part, the result of admixture during flow cytometric isolation (Fig. 6b).

In the CD38⁺ dataset, *TNF* was transcribed by *NCR1*⁺ *GZMB*⁺*CX3CR1*⁺CD56^{dim} NK cells, *GZMB*⁺*CD8B*⁺ effector T cells and CD8⁺ T_{scm} cells (Fig. 6c). Six to eight percent of cells in these clusters transcribed *TNF* at high levels, whereas *TNF* transcription by these cells in control bone marrow was absent or very low (Fig. 6c). *IL1B* transcription was restricted to *LYZ*⁺ myeloid cells, and transcription was similar in individuals with myeloma and non-cancer control patients (Fig. 6d). Next, the non-hematopoietic dataset was merged with either the CD38⁻, CD38⁺*SDC1*⁻ or the CD38⁺*SDC1*⁺ dataset and analyzed for possible receptor–ligand interactions using CellPhoneDB[31]. In line with our expression data, *TNF*-expressing CD38⁻ (Fig. 6e) and CD38⁺ (Fig. 6f) T cells and NK cells were predicted to be able to activate MSC via TNF binding to mesenchymal-expressed *TNFRSF1A* and *TNFRSF1B* encoding TNF-RI and TNF-RII.

Mining non-TNF interactions, we observed iMSC-specific predicted interactions with a subset of myeloma cells. In contrast to VCAM1–$\alpha_4\beta_1$ binding, which appeared to be universal for stromal cell–tumor cell interactions, iMSC cluster MSC1 had the ability to attract myeloma cells via CCL2 signaling (Fig. 7a). This chemokine can either bind CCR10, which was expressed by all myeloma cell clusters (P1–P7), or CCR2, which was predominantly expressed by MM cell cluster P1 (Fig. 7b). CCL2–CCR2 interactions induce proliferation in prostate cancer[32] and breast cancer cells[33]. Befittingly, cluster P1 contained proliferating myeloma cells, as defined by the expression of *MKI67* and genes associated with the G2M/S phase of the cell cycle (Fig. 7c). iMSCs were also predicted to specifically interact with myeloma cells via IL-6–IL-6 receptor interactions (Fig. 7a), a potent stimulus for MM cell survival and proliferation. These findings suggest a possible role for iMSCs in regulating myeloma cell proliferation and indicate that iMSCs might interact with specific subsets of myeloma cells.

The highest number of predicted iMSC–immune cell interactions was with myeloid cells (Fig. 7d). These included iMSC cluster MSC1-specific complement C3 binding to C3AR1 and $\alpha_M\beta_2$ transcribed by monocytes (Fig. 7e–g). MSC-derived complement can regulate immune responses by inhibiting mononuclear cell proliferation[34]. Moreover, both MSC1 and MSC2 were predicted to interact with monocytes via ANXA1 binding to FPR1 or FPR2 (Fig. 7e–g). These receptors serve an anti-inflammatory function by suppressing the production of phospholipase A2, an enzyme involved in inflammatory events, including phagocytosis and respiratory bursts[35]. Intermediate monocytes and CD14⁺ dendritic cells expressed FLT1, one of the receptors for iMSC-derived VEGFA (Fig. 7e–g). Myeloid cells express *TNFSF12* (encoding TWEAK), which can interact with *TNFRSF12A* (TWEAK receptor) specifically expressed on MSC1 and MSC2 (Fig. 7e–g). Myeloid cells also expressed oncostatin M (OSM), which can bind OSMR that is transcribed at higher levels by MSC1 (Fig. 7e). Finally, MSC1- and MSC2-derived IL-6 can interact with myeloid cells expressing the IL-6 receptor (Fig. 7e).

The full CellPhoneDB cellular interaction dataset, including putative reciprocal interactions between bone marrow hematopoietic cells, is available for exploration online (https://github.com/MyelomaRotterdam/Microenvironment).

In sum, these analyses identify *NCR1*⁺*GZMB*⁺*CX3CR1*⁺CD56^{dim} NK cells, *GZMB*⁺*CD8B*⁺ effector T cells and *TNF*⁺*FAS*⁺*GZMK*⁺ T_{scm} cells as potential sources of MSC-activating TNF. Moreover, iMSCs may have the ability to modulate myeloid cell functionality and can specifically interact with proliferating myeloma cells, suggesting iMSCs may play a role in tumor propagation or survival.

Marrow inflammation persists after antitumor therapy. We next set out to determine whether anti-myeloma induction therapy

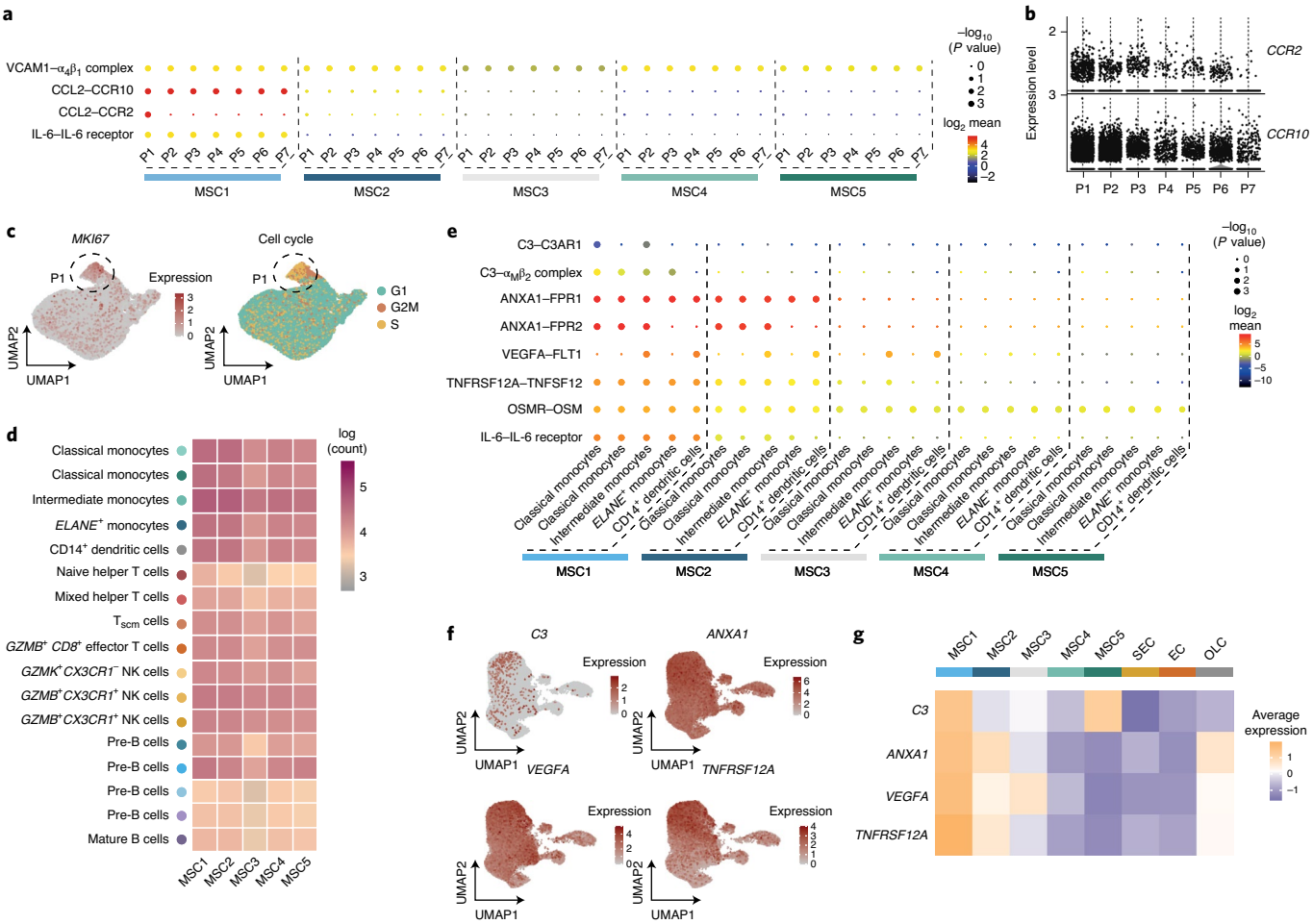

Fig. 7 | Predicted interactions in the myeloma microenvironment. a, Predicted ligand–receptor interactions between MSC clusters and myeloma cell clusters. Means and *P* values were calculated using the statistical framework of CellPhoneDB[31]. **b**, Violin plot of *CCR2* and *CCR10* transcription in myeloma cell clusters. **c**, Transcription of *MKI67* and summarized transcription of cell-cycle-associated genes in the CD38+*SDC1*+ myeloma cell dataset. **d**, Heat map of the number of possible interactions per cluster pair. **e**, Predicted ligand–receptor interactions between MSC clusters and CD38+ myeloid cell clusters. Means and *P* values were calculated using the statistical framework of CellPhoneDB[31]. **f**, Transcription of *C3*, *ANXA1*, *VEGFA* and *TNFRSF12A* in non-hematopoietic cells. **g**, Heat map of average expression of *C3*, *ANXA1*, *VEGFA* and *TNFRSF12A* in non-hematopoietic cell clusters.

could revert bone marrow inflammation. To trace iMSC transcriptomes in individuals during treatment, we first established whether the iMSC signature could be detected by bulk RNA sequencing, as this would allow for the analysis of samples whose cellularity did not permit single-cell RNA sequencing. Hereto, total MSCs from the mononuclear fraction of viably frozen bone marrow aspirates of an additional 14 newly diagnosed individuals with myeloma and 4 aged-matched non-cancer control individuals were isolated by fluorescence-activated cell sorting (for gating strategy, see Extended Data Fig. 1a). Clinical characteristics of all individuals are described in Supplementary Tables 3 and 8. After sequencing, low levels of hematopoietic transcripts were still detected, but these were similar between groups (Extended Data Fig. 7a). Principle component analysis (PCA) showed that MSCs of individuals with myeloma and those of individuals without myeloma were readily distinguished within the first two principle components (PCs) (Fig. 8a). Canonical MSC genes *CXCL12*, *LEPR* and *THY1* (Fig. 8b) and markers of stromal cell subsets *NES*, *PDGFRA*, *PDGFRB*, *ACTA2* and *NGFR* (Extended Data Fig. 7b) were transcribed at equal levels in individuals with myeloma and in non-cancer control patients. A volcano plot of all differentially expressed genes showed a clear difference between individuals with myeloma and control patients, with inflammatory genes demonstrating higher transcription in myeloma MSCs (Fig. 8c). Detailed analyses of inflammatory genes showed increased transcription of most of the previously identified transcripts, with the exception of *CXCL2*, *PTGS1* and *IL1RL1*, which did not reach statistical significance (Fig. 8d). GSEA of the entire set of differentially expressed genes confirmed enrichment for 'TNFα signaling via NFκB' (Fig. 8e), while ECM-associated genes were generally not altered (Extended Data Fig. 7c), again in line with the single-cell data. The top 50 differentially expressed genes between myeloma and control MSCs are detailed in Supplementary Table 12.

For 9 of the 14 individuals, paired frozen bone marrow aspirates after four courses (4×28 d) of induction treatment were available (see Supplementary Tables 9 and 11 for clinical characteristics and types of treatment). After induction therapy, three of nine individuals were minimal residual disease negative (MRD^{neg}) as determined by flow cytometry (at a sensitivity threshold of 10^{-5}), while six of nine individuals still had detectable tumor load (MRD^{pos}). RNA sequencing of sort-purified MSCs revealed that the general MSC transcriptome was unaltered by induction therapy, with the exception of slightly more T cell admixture after therapy (Extended Data Fig. 7d–f), and a PCA showed no separate clustering of samples based on timing of sample collection (Fig. 8f). Analysis of differentially expressed genes revealed only a small number of altered genes

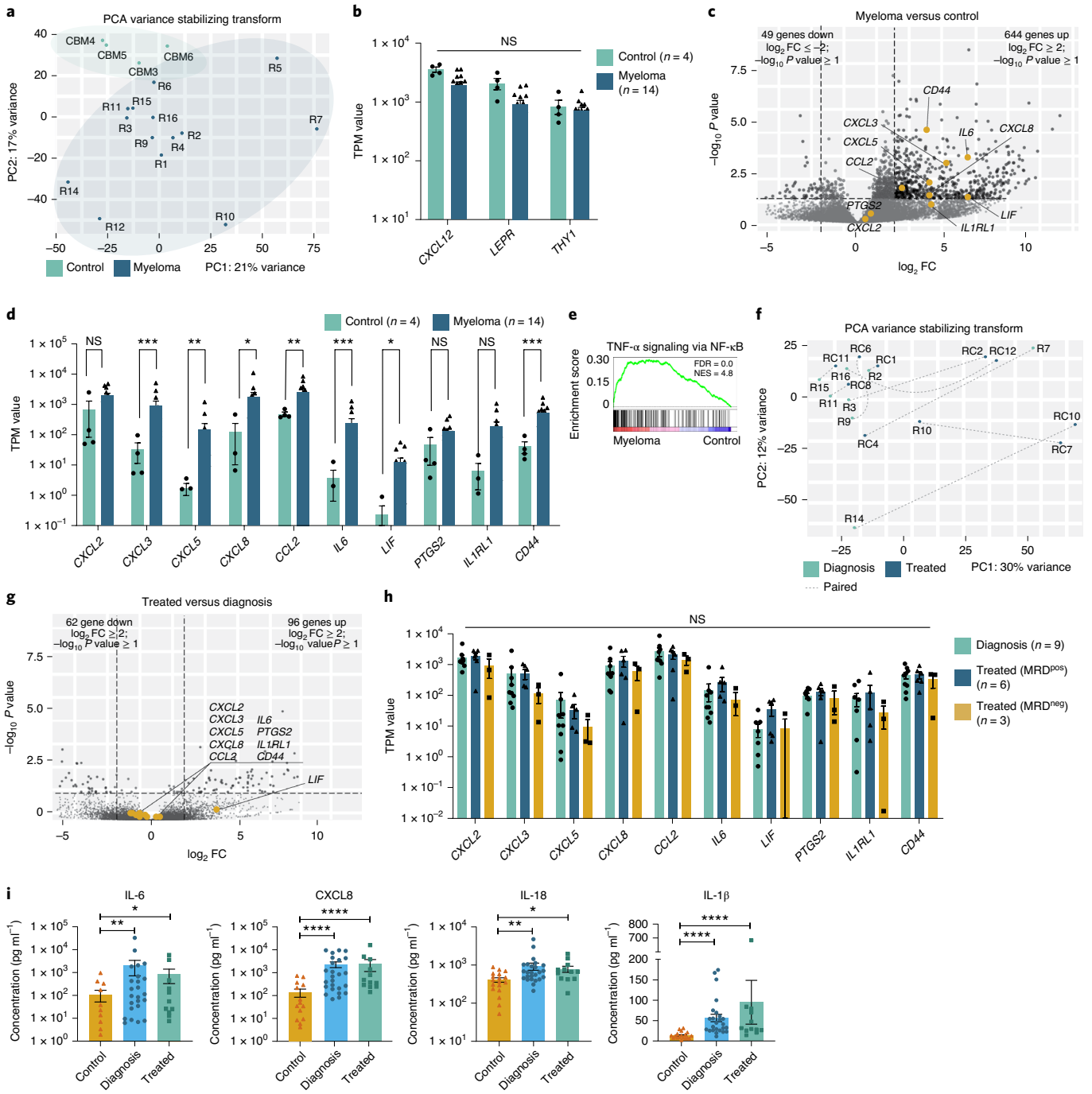

Fig. 8 | Bone marrow inflammation persists after successful antitumor therapy. a, PCA of bulk RNA sequencing of purified MSCs showing the coordinates of samples from individuals with myeloma ($n = 14$, blue) and individuals without myeloma ($n = 4$, green). **b**, Transcription of canonical MSC marker genes comparing the myeloma dataset (blue) to the non-myeloma dataset (green). **c**, Volcano plot depicting differentially expressed genes in the myeloma dataset versus in the control dataset; $\log_2$ fold change (FC) cutoff, 2; $-\log_{10} P$ value, 1. **d**, Transcription of inflammatory genes comparing the myeloma dataset (blue) to the non-myeloma control dataset (green). Dots represent individuals. **e**, GSEA enrichment plot for gene set 'TNFα signaling via NFκB' in myeloma samples as compared to control samples; FDR, false discovery rate; NES, normalized enrichment score. **f**, PCA of bulk RNA sequencing of purified MSCs showing the coordinates of samples from newly diagnosed individuals with myeloma ($n = 9$, green) and samples taken after induction treatment ($n = 9$, blue). Dotted lines represent paired samples from the same individual. **g**, Volcano plot depicting differentially expressed genes in samples taken after induction treatment versus samples taken at diagnosis; $\log_2$ FC cutoff, 2; $-\log_{10} P$ value, 1. **h**, Transcription of inflammatory genes at diagnosis (green) as compared to post-induction treatment in MRD^{pos} individuals ($n = 6$, blue) or MRD^{neg} individuals ($n = 3$, yellow). Dots represent individuals. **i**, Bar graphs depicting IL-6, CXCL8, IL-18 and IL-1β protein levels in the bone marrow plasma of newly diagnosed individuals with myeloma ($n = 25$), individuals after induction treatment ($n = 12$) and healthy participants ($n = 18$) (control and diagnosis for IL-6 and CXCL8 from Fig. 1j and for IL-1β from Fig. 3d). The data in **b**,**c**,**d**,**g**,**h** and **i** are presented as mean ± s.e.m. For **b**,**c**,**d**,**g** and **h**, significance was calculated using the Wald test (two-tailed) followed by a Benjamini–Hochberg correction. Significance for **i** was calculated using the Mann–Whitney *U* test (two-tailed); $^*P \leq 0.05$, $^{**}P \leq 0.01$, $^{***}P \leq 0.001$, $^{****}P \leq 0.0001$. TPM, transcripts per million.

after induction therapy (Supplementary Table 13). In particular, the inflammatory iMSC transcriptome was unaltered after induction therapy, even if individuals had reached MRD negativity (Fig. 8g,h).

Inflammatory proteins that were significantly elevated in bone marrow plasma at diagnosis compared to non-myeloma control samples, including IL-1β, remained elevated after induction therapy, as did other markers of inflammation, such as IL-18 (Fig. 8i). In conclusion, MM-associated inflammatory changes in the bone marrow microenvironment persist even after successful antitumor induction therapy and warrant further studies into the role of protumor inflammation in MM pathobiology and disease relapse.

Discussion

The importance of the non-malignant microenvironment in cancer pathobiology is increasingly appreciated, and local, often low-grade, subclinical inflammation is an important driver of tumor development, growth and therapy resistance in various malignancies[36]. Bone marrow MSCs are considered important drivers of myeloma pathobiology; yet, how the stromal backbone of the bone marrow is rewired to accommodate tumor residence remained unclear. Here, we present a combined single-cell transcriptomic analysis of the hematopoietic and non-hematopoietic bone marrow microenvironment in MM and provide evidence for MSC-centric bone marrow inflammation, creating an environment poised for tumor cell proliferation and immune cell modulation.

iMSCs were the result of NF-κB-mediated activation of MSCs, possibly via TNF or IL-1β. IL-1β protein was significantly elevated in myeloma bone marrow supernatants, but frequencies of *IL1B*-expressing cell populations in bone marrow aspirates did not differ from those found in individuals without myeloma. Of note, polynuclear myeloid cells, which are dominant sources of IL-1β, were not included in our sequencing experiments, and IL-1β secretion is regulated post-transcriptionally[37]. We identified three *TNF*-transcribing immune cell subsets: *NCR1*$^{+}$*GZMB*$^{+}$*CX3CR1*$^{+}$CD56^{dim} NK cells, *IFIT1*$^{+}$*IFIT2*$^{+}$*IFIT3*$^{+}$ IFN-responsive T cells and *CD8B*$^{+}$*TNF*$^{+}$*FAS*$^{+}$*GZMK*$^{+}$ T_{scm} cells, of which the latter two populations were increased in individuals with MM compared to non-cancer control individuals. We hypothesize that tumor cells present in the bone marrow either activate MSCs directly or evoke chronic immune activation, leading to the production of inflammatory cytokines that can activate bone marrow MSCs[38]. Activated iMSCs transcribed genes involved in the direct modulation of T cell responses, including *PTGS2* (encoding COX-2). COX-2 is a rate-limiting enzyme during prostaglandin biosynthesis[39], and stromal cell-derived PGE_2 can inhibit T cell responses[22,40]. iMSCs also transcribed genes with the ability to modulate myeloid cell function, including *C3* and *ANXA1*. At least part of the iMSCs transcribed *CD44*, a marker associated with cancer-associated fibroblasts (CAFs) in solid tumors[41,42]. Myeloma iMSCs show similarities to the inflammatory CAF subset, which favors differentiation and recruitment of tolerogenic immune cells, such as MDSCs[43], via the production of CXCR1/CXCR2 ligands and IL-6 (refs. [20,44,45]). Based on the iMSC transcriptome and predicted putative interactions, iMSCs may act as both survival and proliferation niches for MM cells and simultaneously recruit and modulate immune cells (summarized in a hypothetical model in Extended Data Fig. 8). Mechanistic experiments will be essential to validate these hypotheses.

We focused on TNF–TNF receptor and IL-1β–IL-1 receptor interactions as potential NF-κB stimuli leading to iMSC activation. This notwithstanding, NF-κB signaling can be induced by various external signals, including multiple types of pattern recognition receptors (PRRs)[46]. PRRs can bind damage-associated molecular patterns (DAMPs), such as nuclear or cytosolic proteins released following cell death or peptides derived from ECM breakdown[47]. Hypoxic conditions and increasing tumor bulk in the myeloma bone marrow disrupts bone marrow homeostasis and anatomy, resulting in massive release of DAMPs[48], while myeloma cells themselves can secrete exosomes containing DAMPs[49]. Activation of iMSCs may thus not only result from TNF and/or IL-1β stimulation but also could be downstream of PRR–DAMP interactions.

In situ, CD44^{+} iMSCs were found scattered throughout the bone marrow, interacting with MM cells and T cells. Importantly, no 'pan-iMSC' marker has been identified in our studies. CD44 does not label all iMSCs, and our histological analyses likely only identified cells expressing the highest levels of CD44. More elaborate multiplex immunohistology will be required to fully chart iMSC cellular interactions in MM bone marrow.

In the cohort that we followed over time, four courses of induction therapy did not normalize bone marrow mesenchymal cell inflammation, not even in individuals whose tumor became undetectable by flow cytometry. A possible explanation would be the continued presence of inflammatory immune cells, which was supported by the continued increased levels of IL-1β and other inflammatory proteins after induction therapy. Alternatively, prolonged iMSC activation may also lead to more fundamental epigenetic changes in the stromal backbone of the marrow, which persists even in the absence of tumor cells.

In summary, our work provides the identification of myeloma-specific bone marrow MSCs and reveals the presence of bone marrow inflammation persisting even after successful induction therapy. In addition, we provide a single-cell transcriptomic analysis of the human non-hematopoietic bone marrow niche paired with hematopoietic and tumor cells in newly diagnosed MM. Our findings warrant further investigation into the initiation and maintenance of bone marrow inflammation during MM development, treatment and relapse. The resources generated in this study can serve as a blueprint for the identification of iMSCs in other bone marrow malignancies, especially those associated with inflammatory features, such as myelodysplastic syndrome (MDS)–acute myeloid leukemia (AML)[50]. Moreover, alignment of bone marrow iMSC transcriptomes with inflammatory CAFs in solid tumors[42] will be an important step toward the identification of possible mechanistic commonalities in niche alterations and protumor inflammation across malignancies.

Online content

Any methods, additional references, Nature Research reporting summaries, source data, extended data, supplementary information, acknowledgements, peer review information; details of author contributions and competing interests; and statements of data and code availability are available at https://doi.org/10.1038/s41590-021-00931-3.

Received: 25 June 2020; Accepted: 9 April 2021;
Published online: 20 May 2021

References

1. Scrivo, R., Vasile, M., Bartosiewicz, I. & Valesini, G. Inflammation as 'common soil' of the multifactorial diseases. *Autoimmun. Rev.* **10**, 369–374 (2011).
2. Lomas, O. C., Tahri, S. & Ghobrial, I. M. The microenvironment in myeloma. *Curr. Opin. Oncol.* **32**, 170–175 (2020).
3. Monteran, L. & Erez, N. The dark side of fibroblasts: cancer-associated fibroblasts as mediators of immunosuppression in the tumor microenvironment. *Front. Immunol.* **10**, 1835 (2019).
4. Baryawno, N. et al. A cellular taxonomy of the bone marrow stroma in homeostasis and leukemia. *Cell* **177**, 1915–1932 (2019).
5. Helbling, P. M. et al. Global transcriptomic profiling of the bone marrow stromal microenvironment during postnatal development, aging, and inflammation. *Cell Rep.* **29**, 3313–3330 (2019).
6. Cassese, G. et al. Plasma cell survival is mediated by synergistic effects of cytokines and adhesion-dependent signals. *J. Immunol.* **171**, 1684–1690 (2003).
7. Corre, J. et al. Bone marrow mesenchymal stem cells are abnormal in multiple myeloma. *Leukemia* **21**, 1079–1088 (2007).

8. Ghobrial, I. M., Detappe, A., Anderson, K. C. & Steensma, D. P. The bone-marrow niche in MDS and MGUS: implications for AML and MM. *Nat. Rev. Clin. Oncol.* **15**, 219–233 (2018).
9. Das, R. et al. Microenvironment-dependent growth of preneoplastic and malignant plasma cells in humanized mice. *Nat. Med.* **22**, 1351–1357 (2016).
10. Zavidij, O. et al. Single-cell RNA sequencing reveals compromised immune microenvironment in precursor stages of multiple myeloma. *Nat. Cancer* **1**, 493–506 (2020).
11. Bailur, J. K. et al. Early alterations in stem-like/resident T cells, innate and myeloid cells in the bone marrow in preneoplastic gammopathy. *JCI Insight* **5**, e127807 (2019).
12. Görgün, G. T. et al. Tumor-promoting immune-suppressive myeloid-derived suppressor cells in the multiple myeloma microenvironment in humans. *Blood* **121**, 2975–2987 (2013).
13. Favaloro, J. et al. Myeloid derived suppressor cells are numerically, functionally and phenotypically different in patients with multiple myeloma. *Leuk. Lymphoma* **55**, 2893–2900 (2014).
14. Nooka, A. K. et al. Daratumumab in multiple myeloma. *Cancer* **125**, 2364–2382 (2019).
15. Moreau, P. et al. Bortezomib, thalidomide, and dexamethasone with or without daratumumab before and after autologous stem-cell transplantation for newly diagnosed multiple myeloma (CASSIOPEIA): a randomised, open-label, phase 3 study. *Lancet* **394**, 29–38 (2019).
16. Kumar, S. K. et al. Multiple myeloma. *Nat. Rev. Dis. Prim.* **3**, 17046 (2017).
17. Barrionuevo, N., Gatica, S., Olivares, P., Cabello-Verrugio, C. & Simon, F. Endothelial cells exhibit two waves of P-selectin surface aggregation under endotoxic and oxidative conditions. *Protein J.* **38**, 667–674 (2019).
18. Barut, B. A. et al. Role of interleukin 6 in the growth of myeloma-derived cell lines. *Leuk. Res.* **16**, 951–959 (1992).
19. Nishimoto, N. et al. Oncostatin M, leukemia inhibitory factor, and interleukin 6 induce the proliferation of human plasmacytoma cells via the common signal transducer, gp130. *J. Exp. Med.* **179**, 1343–1347 (1994).
20. Alfaro, C. et al. Tumor-produced interleukin-8 attracts human myeloid-derived suppressor cells and elicits extrusion of neutrophil extracellular traps (NETs). *Clin. Cancer Res.* **22**, 3924–3936 (2016).
21. Shi, H. et al. Chemokine (C-X-C motif) ligand 1 and CXCL2 produced by tumor promote the generation of monocytic myeloid-derived suppressor cells. *Cancer Sci.* **109**, 3826–3839 (2018).
22. Schaeuble, K. et al. Attenuation of chronic antiviral T-cell responses through constitutive COX2-dependent prostanoid synthesis by lymph node fibroblasts. *PLoS Biol.* **17**, e3000072 (2019).
23. Molejon, M. I. et al. Deciphering the cellular source of tumor relapse identifies CD44 as a major therapeutic target in pancreatic adenocarcinoma. *Oncotarget* **6**, 7408–7423 (2015).
24. Yang, C. et al. Inducible formation of leader cells driven by CD44 switching gives rise to collective invasion and metastases in luminal breast carcinomas. *Oncogene* **38**, 7113–7132 (2019).
25. Filippi, I. et al. Different adaptive responses to hypoxia in normal and multiple myeloma endothelial cells. *Cell. Physiol. Biochem.* **46**, 203–212 (2018).
26. Kang, H. S. et al. CD44 plays a critical role in regulating diet-induced adipose inflammation, hepatic steatosis, and insulin resistance. *PLoS ONE* **8**, e58417 (2013).
27. Szklarczyk, D. et al. STRING v11: protein–protein association networks with increased coverage, supporting functional discovery in genome-wide experimental datasets. *Nucleic Acids Res.* **47**, D607–D613 (2019).
28. Hideshima, T., Chauhan, D., Schlossman, R., Richardson, P. & Anderson, K. C. The role of tumor necrosis factor α in the pathophysiology of human multiple myeloma: therapeutic applications. *Oncogene* **20**, 4519–4527 (2001).
29. Morris, E. V. et al. Myeloma cells down-regulate adiponectin in bone marrow adipocytes via TNF-α. *J. Bone Miner. Res.* **35**, 942–955 (2020).
30. Gars, M. L. et al. CD38 contributes to human natural killer cell responses through a role in immune synapse formation. Preprint at *bioRxiv*, https://doi.org/10.1101/349084 (2019).
31. Efremova, M., Vento-Tormo, M., Teichmann, S. A. & Vento-Tormo, R. CellPhoneDB: inferring cell–cell communication from combined expression of multi-subunit ligand–receptor complexes. *Nat. Protoc.* **15**, 1484–1506 (2020).
32. Loberg, R. D. et al. CCL2 is a potent regulator of prostate cancer cell migration and proliferation. *Neoplasia* **8**, 578–586 (2006).
33. Chen, X. et al. CCL2/CCR2 regulates the tumor microenvironment in HER-2/neu-driven mammary carcinomas in mice. *PLoS ONE* **11**, e0165595 (2016).
34. Moll, G. et al. Mesenchymal stromal cells engage complement and complement receptor bearing innate effector cells to modulate immune responses. *PLoS ONE* **6**, e21703 (2011).
35. Perretti, M. & D'Acquisto, F. Annexin A1 and glucocorticoids as effectors of the resolution of inflammation. *Nat. Rev. Immunol.* **9**, 62–70 (2009).
36. Diakos, C. I., Charles, K. A., McMillan, D. C. & Clarke, S. J. Cancer-related inflammation and treatment effectiveness. *Lancet Oncol.* **15**, e493–e503 (2014).
37. Rubartelli, A., Bajetto, A., Allavena, G., Cozzolino, F. & Sitia, R. Post-translational regulation of interleukin 1β secretion. *Cytokine* **5**, 117–124 (1993).
38. Erez, N., Truitt, M., Olson, P. & Hanahan, D. Cancer-associated fibroblasts are activated in incipient neoplasia to orchestrate tumor-promoting inflammation in an NF-κB-dependent manner. *Cancer Cell* **17**, 135–147 (2010).
39. Tong, D. et al. The roles of the COX2/PGE2/EP axis in therapeutic resistance. *Cancer Metastasis Rev.* **37**, 355–368 (2018).
40. Li, A., Chen, P., Leng, Y. & Kang, J. Histone deacetylase 6 regulates the immunosuppressive properties of cancer-associated fibroblasts in breast cancer through the STAT3–COX2-dependent pathway. *Oncogene* **37**, 5952–5966 (2018).
41. Santi, A., Kugeratski, F. G. & Zanivan, S. Cancer associated fibroblasts: the architects of stroma remodeling. *Proteomics* **18**, e1700167 (2018).
42. Miyai, Y., Esaki, N., Takahashi, M. & Enomoto, A. Cancer-associated fibroblasts that restrain cancer progression: hypotheses and perspectives. *Cancer Sci.* **111**, 1047–1057 (2020).
43. Liu, T. et al. Cancer-associated fibroblasts: an emerging target of anti-cancer immunotherapy. *J. Hematol. Oncol.* **12**, 86 (2019).
44. Zhang, H. et al. CXCL2/MIF–CXCR2 signaling promotes the recruitment of myeloid-derived suppressor cells and is correlated with prognosis in bladder cancer. *Oncogene* **36**, 2095–2104 (2017).
45. Tobin, R. P. et al. IL-6 and IL-8 are linked with myeloid-derived suppressor cell accumulation and correlate with poor clinical outcomes in melanoma patients. *Front. Oncol.* **9**, 1223 (2019).
46. Kumar, H., Kawai, T. & Akira, S. Pathogen recognition by the innate immune system. *Int. Rev. Immunol.* **30**, 16–34 (2011).
47. Amarante-Mendes, G. P. et al. Pattern recognition receptors and the host cell death molecular machinery. *Front. Immunol.* **9**, 2379 (2018).
48. Hope, C. et al. Immunoregulatory roles of versican proteolysis in the myeloma microenvironment. *Blood* **128**, 680–685 (2016).
49. Vulpis, E. et al. Genotoxic stress modulates the release of exosomes from multiple myeloma cells capable of activating NK cell cytokine production: role of HSP70/TLR2/NF-kB axis. *Oncoimmunology* **6**, e1279372 (2017).
50. Ping, Z. et al. Activation of NF-κB driven inflammatory programs in mesenchymal elements attenuates hematopoiesis in low-risk myelodysplastic syndromes. *Leukemia* **33**, 536–541 (2019).

Methods

Sample acquisition. Paired bone marrow aspirates from individuals with myeloma at diagnosis and after induction treatment were obtained from individuals included in a large multicenter, prospective, randomized phase 3 trial Cassiopeia (Dutch-Belgian Cooperative Trial Group for Hemato-Oncology [HOVON]131/Intergroupe Francophone du Myeloma (IFM) 2015-01; ClinicalTrials.gov identifier NCT02541383) or collected as part of routine diagnostics at the Erasmus MC or Universitäts Klinikum Münster. Control marrow was obtained by sternal aspiration from donors undergoing cardiothoracic surgery or by manual bone marrow collection from femur heads collected after hip replacement surgery. All material was obtained after written informed consent approved by the Institutional Review Boards of the Erasmus Medical Center (Rotterdam, the Netherlands) or Universitäts Klinikum Münster (Münster, Germany) in accordance with the Declaration of Helsinki. Marrow aspirates were used within 24 h after collection, with the exception of three samples that were used after 48 h (PT1, PT2 and R7). Mononuclear cell fractions were isolated using Histopaque (Sigma-Aldrich), and plasma cells were purified using the EasySep human CD138 Positive Selection kit II (Stemcell). The mononuclear cell fractions, plasma cell fractions and negative fractions after purification were viably frozen in Dulbecco's modified eagle medium (DMEM; Gibco) supplemented with 40% heat-inactivated fetal calf serum (FCS; Corning) and 10% dimethyl sulfoxide (DMSO; Sigma-Aldrich). All participant characteristics are detailed in Supplementary Tables 1–3 and 8–11.

Isolation of non-hematopoietic and hematopoietic cells for transcriptomic analyses. Viably frozen bone marrow aspirates were thawed in DMEM supplemented with 10% FCS according to the 10x Genomics protocol 'Fresh Frozen Human Peripheral Blood Mononuclear Cells for Single-cell RNA sequencing'. For non-hematopoietic cell isolation, only samples containing $>200\times10^6$ mononuclear cells were included for sequencing studies. Fc receptors were blocked with 10% normal human AB serum (Sigma-Aldrich). To enrich for MSCs, samples were incubated with biotinylated antibodies against CD45 (1:50, clone HI30; BioLegend), CD235a (1:50, clone HIR2; BioLegend) and CD38 (20 µl per 10^7 cells, from human CD38 MicroBead kit; Miltenyi Biotec) followed by depletion using magnetic anti-biotin beads (30 µl per 10^7 cells; Miltenyi Biotec) and the iMag (BD Biosciences). After depletion, cells were stained for sorting in PBS containing 2% FCS at 4 °C with the following antibodies: CD271-PE (1:200; ME20.4, BioLegend), CD235a-PECy7 (1:20; HI264, BioLegend), CD31-APCCy7 (1:20; WM59, BioLegend), CD44-BV711 (1:50; IM7, BioLegend), streptavidin-BV421 (1:200; BioLegend), CD34-PECF610 (1:100; 4H11, eBioscience), CD45-APC (1:20; 2D1, eBioscience), CD38-FITC (1:20; MHCD3801, Life Technologies), CD71-Alexa Fluor 700 (1:20; MEM-75, ExBio) and CD105-BV510 (1:50; 266, BD Biosciences). For dead cell exclusion, 7AAD (1:100; Beckman Coulter) or DAPI (1:100; Life Technologies) was used. For single-cell sequencing studies, $CD45^-CD38^-CD235a^-CD71^-$ non-hematopoietic cells were sorted in DMEM supplemented with 10% FCS using a FACSAria III (BD Biosciences) and BD FACSDiva version 5.0. Before depletion, 10×10^6 cells were used to sort $CD45^+CD38^-CD34^-CD235a^-CD71^-$ and $CD38^+CD34^-CD235a^-CD71^-$ hematopoietic populations using the same antibody panel.

For bulk sequencing studies, $CD45^-CD38^-CD235a^-CD71^-CD31^-$ non-hematopoietic cells were directly sorted in lysis buffer containing TCEP (Macherey-Nagel) using a FACSAria III (BD BioSciences). See Extended Data Fig. 1a,c for sorting strategies.

For purification of cells for qPCR analysis of TNF and IL-1β, cells were stained in PBS containing 2% FCS at 4 °C with the following antibodies: CD45-BV510 (1:50; HI30, Sony Biotechnology), CD14-PECy7 (1:20; HCD14, BioLegend), CD138-PECF594 (1:100; MI15, BD Biosciences) and CD235a-APC (1:50; GA-R2, BD Biosciences). DAPI (1:100; Life Technologies) was used for dead cell exclusion. Cells were directly sorted in lysis buffer containing TCEP (Macherey-Nagel) using a FACSAria III (BD Biosciences) and BD FACSDiva version 5.0. See Extended Data Fig. 2b for sorting strategy. $CD138^+$ myeloma cells were obtained using the EasySep human CD138 Positive Selection kit II (Stemcell) on fresh material.

For purification of cells for qPCR analysis of *GZMB* and *GZMK*, cells were stained in PBS containing 2% FCS at 4 °C with the following antibodies: CD95-APC (1:20; DX2, BD Pharmingen), CD45RA-APC-H7 (1:50; HI100, BD Pharmingen), CD3-Alexa Fluor 700 (1:100; UCHT1, BD Pharmingen), CD122-PerCP-Cy5.5 (1:20; TU27, BioLegend), CD27-PE Dazzle 594 (1:100; M-T271, BioLegend), CD56-PECy7 (1:50; CMSSB, eBioscience), CD38-PE (1:100; HB-7, BD Biosciences) and CD8-FITC (1:100; MEM-31, ImmunoTools). DAPI (1:100; Life Technologies) was used for dead cell exclusion. Cells were directly sorted in lysis buffer containing TCEP (Macherey-Nagel) using a FACSAria III (BD Biosciences) and BD FACSDiva version 5.0. See Extended Data Fig. 4b for sorting strategy.

Single-cell RNA sequencing. Single cells were encapsulated for cDNA synthesis and barcoded using the Chromium Single-cell 3′ Reagent kit v3 (10x Genomics) followed by library construction according to the manufacturer's recommendations. Sorted non-hematopoietic cells were combined with sorted $CD45^+CD38^-CD34^-CD235a^-CD71^-$ hematopoietic cells and processed as one sample. The quality and quantity of libraries was determined using an Agilent 2100 Bioanalyzer with 2100 Expert version B.02.11.SI811 software and a High Sensitivity DNA kit. Libraries were sequenced on a NovaSeq 6000 platform (Illumina), paired-end mode, at a sequencing depth of ~20,000 reads per cell, followed by computational alignment using CellRanger (version 3.0.2, 10x Genomics). Subsequently, datasets were subjected to quality control steps using Seurat (R package, version 3.1.0 and version 4.0.0)[51] that included selecting cells with a library complexity of more than 200 features, removing doublets (cells with double amounts of unique molecular identifiers (UMIs)) and filtering out cells with high percentages of mitochondrial genes (>10%) (script available at https://github.com/MyelomaRotterdam/Microenvironment). In the *CD38*$^+$ dataset, Ig genes were removed before downstream analyses. Non-hematopoietic cells expressing *CXCL12* (MSCs) and/or *CD36* (endothelial cells) and $CD45^+CD38^-$ hematopoietic cells were separated in silico using Seurat's CellSelector tool. Clusters containing *SDC1*$^+$ plasma cells were separated from other $CD38^+$ cells using the subset() function and analyzed as an independent dataset to increase resolution. For identification of cell subsets, data from samples from 13 individuals with myeloma and from 7 (non-hematopoietic dataset) or 5 (hematopoietic datasets) individuals without myeloma were merged by integration and label transfer[52], normalized and analyzed by PCA on the most variable genes ($k=2{,}000$) across all cells. With the PCs ($k=10$–20), unsupervised clustering was performed using a shared nearest neighbor (SNN) modularity optimization-based clustering algorithm (resolution 0.3–1) integrated in Seurat[53], and cells were projected in two dimensions using UMAP[54]. Gene set enrichments were calculated with GSEA software (Broad Institute) using the predefined gene sets from the Molecular Signatures Database (MSigDB 6.2)[55,56]. The gene lists were ranked according to $\log_2$FC from the FindMarkers function, and the preranked GSEA was run using the classic enrichment statistic with 1,000 permutations. Pseudotime analysis was carried out using Monocle 3 (ref. [57]). Receptor–ligand interactions were mapped by CellPhoneDB[31] using a threshold of 0.03 after merging the non-hematopoietic dataset with the $SDC1^+CD38^+$, $SDC1^-CD38^+$ or $CD38^-$ datasets and normalization via Seurat's NormalizeData() function using the 'RC' method.

Bulk RNA sequencing. RNA was extracted using the NucleoSpin RNA XS kit (Macherey-Nagel). cDNA was prepared using the SMARTer Ultra Low RNA kit for Illumina Sequencing (Clontech Laboratories) according to the manufacturer's protocol. The quality and quantity of cDNA samples was verified using the Agilent 2100 Bioanalyzer with 2100 Expert Software version B.02.11.SI811 and the High Sensitivity DNA kit. cDNA libraries were generated using the TruSeq Sample Preparation v2 guide (Illumina) and paired-end-sequenced on a NovaSeq 6000 (Illumina) (median read length, 362 ± 52 base pairs). Adaptor sequences and polyT tails were trimmed from unprocessed reads with fqtrim version 0.9.7. (http://ccb.jhu.edu/software/fqtrim/). Read counts and TPM were determined with Salmon version 1.2.1 (ref. [58]). Gene count estimates were determined from Salmon output in combination with the tximport R package version 1.16 (ref. [59]). These gene count estimates were in turn normalized, prefiltered according to standard practice and used for determining the differential expression of genes between groups of interest through the DESeq2 package[60] (version 1.28) using default parameters. GSEA was performed with GSEA software (version 3.0, Broad Institute) using predefined gene sets from the Molecular Signatures Database (MSigDB 6.2). Gene lists were ranked on the basis of the $\log_2$FC or the ashr method[61] made available through the DESeq2 package. Classical enrichment statistics with 1,000 permutations was used to determine significant enrichment within gene sets.

Stimulation cultures. Primary myeloma MSCs from bone marrow aspirates and primary control MSCs from femur heads were obtained by culture of erythrocyte-lysed bone marrow aspirates in MesenPro RS medium (Gibco) supplemented with 2 mM glutaMAX (Gibco) and 1% penicillin/streptomycin (Sigma-Aldrich). Supernatant was removed and replaced with fresh medium twice weekly. Adherent cells were cultured for 2–5 passages before use. For stimulation experiments, 50,000 cells were seeded in 12-well plates (approximately confluent) in DMEM supplemented with 10% FCS and stimulated with rhTNF (2.5 ng ml^{-1}; R&D Systems) or rhIL-1β (5 ng ml^{-1}; Miltenyi Biotec) for 24 h. After trypsinization (0.05% Trypsin/EDTA, Gibco), cells were directly lysed in lysis buffer containing TCEP (Macherey-Nagel) and stored at −80 °C until further processing.

Cytokine–Chemokine analysis. Bone marrow plasma was collected from bone marrow aspirates after ficoll separation and stored at −80 °C until use. Before proteomic analyses, supernatant vials were centrifuged twice at 21,000*g* for 5 min to pellet and discard lipid contents, debris and residual cells. Cytokine concentrations were determined using the LegendPlex human inflammation panel 1 (BioLegend) with the LegendPlex Data Analysis Software Suite version 2020.12.15, and IL-1β concentrations were determined using the Human IL-1β/IL-1F2 Quantikine HS ELISA kit (R&D Systems) with the Perkin Elmer VICTOR X4 Multilabel Plate reader, according to the manufacturer's recommendations.

Flow cytometry. Viably frozen bone marrow aspirates were thawed in DMEM supplemented with 10% FCS according to the 10x Genomics protocol 'Fresh Frozen Human Peripheral Blood Mononuclear Cells for Single-cell RNA sequencing'. Fc receptors were blocked with 10% normal human AB serum (Sigma-Aldrich). For quantitative analysis of $CD44^+$ iMSCs, cells were stained

in PBS containing 2% FCS at 4 °C with the following antibodies: CD235a-PECy7 (1:20; HI264, BioLegend), CD31-APCCy7 (1:20; WM59, BioLegend), CD44-BV711 (1:50; IM7, BioLegend), streptavidin-BV421 (1:200; BioLegend), CD34-PECF610 (1:100; 4H11, eBioscience), CD45-APC (1:20; 2D1, eBioscience), CD38-FITC (1:20; MHCD3801, Life Technologies), CD71-Alexa Fluor 700 (1:20; MEM-75, ExBio) and CD105-BV510 (1:50; 266, BD Biosciences). For dead cell exclusion, DAPI (1:100; Life Technologies) was used. Events were acquired on a FACSAria III (BD BioSciences) using BD FACSDiva version 5.0. See Extended Data Fig. 4a for gating strategy. Analyses were carried out using FlowJo version 10.6.1 (BD).

For quantitative analysis of T_{scm} cell and CD56^{bright} NK cell populations, cells were stained in PBS containing 2% FCS at 4 °C with the following antibodies: CD95-APC (1:20; DX2, BD Pharmingen), CD45RA-APC-H7 (1:50; HI100, BD Pharmingen), CD3-Alexa Fluor 700 (1:100; UCHT1, BD Pharmingen), CD122-PerCP-Cy5.5 (1:20; TU27, BioLegend), CD27-PE Dazzle 594 (1:100; M-T271, BioLegend), CD56-PECy7 (1:50; CMSSB, eBioscience), CD38-PE (1:100; HB-7, BD Biosciences) and CD8-FITC (1:100; MEM-31, ImmunoTools). For dead cell exclusion, DAPI (1:100; Life Technologies) was used. Events were acquired on a FACSAria III (BD Biosciences) using BD FACSDiva version 5.0. Analyses were carried out using FlowJo version 10.6.1 (BD). The gating strategies are depicted in Extended Data Fig. 4b. Percentages of CD38$^+$CD3$^+$CD8$^+$CD45RA$^+$CD27$^+$FAS$^+$ T_{scm} cells were calculated as fractions of CD38$^+$CD3$^+$CD8$^+$ T cells, and percentages of CD38$^+$CD56^{bright} and CD38$^+$CD56^{bright}CD27$^+$ NK cells were calculated as fractions of CD38$^+$CD56$^+$ NK cells. See Extended Data Fig. 4c for gating strategy.

Transcript analyses. RNA was extracted using the NucleoSpin RNA XS kit (Macherey-Nagel). cDNA was generated using the SensiFast cDNA synthesis kit (BioLine). For qPCR, a Neviti thermal cycler (Applied Biosystems) and DyNAmo Flash SYBR Green qPCR kit (Finnzymes) were used with the addition of $MgCl_2$ to a final concentration of 4 mM. All reactions were performed in duplicate and were normalized to the expression of *GAPDH*. Relative expression was calculated by the cycling threshold (C_t) method as $-2^{\Delta C_t}$. Primer sequences were as follows: *GAPDH* (forward, 5′-GTCGGAGTCAACGGATT-3′; reverse, 5′-AAGCTTCCCGTTCTCAG-3′), *LEPR* (forward, 5′-CTGCTGCAA TGAACATGA-3′; reverse, 5′-GGCTGCTCCTATGATACCT-3′), *CXCL2* (forward, 5′-GGGAATTCACCTCAAGAAC-3′; reverse, 5′-GGATTT GCCATTTTTCAG-3′), *CXCL3* (forward, 5′-GCAGGGAATTCACCTCA-3′; reverse, 5′-GTGCTCCCCTTGTTCAG-3′), *CXCL8* (forward, 5′-TGCCAAGGA GTGCTAAAG-3′; reverse, 5′-TTGGGGTCCAGACAGAG-3′), *IL6* (forward, 5′-CCCCCAGGAGAAGATTC-3′; reverse, 5′-GCTGCTTTCACACATGTT ACT-3′), *LIF* (forward, 5′-GCCAATGCCCTCTTTATT-3′; reverse, 5′-GGAGG TGCCAAGGTACA-3′), *PTGS2* (forward, 5′-TGGGGTGGACTTAAATCA-3′; reverse, 5′-TGAGGAGGGTAGATCATCT-3′), *CD44* (forward, 5′-AACGAATC CTGAAGACATCTAC-3′; reverse, 5′-GCAGGGATTCTGTCTGTG-3′), *TNF* (forward, 5′-CGCTCCCCAAGAAGAC-3′; reverse, 5′-AGGGCTGATTAGAG AGAGGT-3′), *IL1B* (forward, 5′-CCTGCCCACAGACCT-3′; reverse, 5′-GG ACCAGACATCACCAAG-3′), *GZMK* (forward, 5′-ACCCTGCGAGAAG TCAC-3′; reverse, 5′-GCGTGGAAGACACCTTT-3′) and *GZMB* (forward, 5′-TGGGGAAGCTCCATAAA-3′; reverse, 5′-GGGCCTTGTTGCTAGG-3′).

Immunohistochemistry. Bone marrow biopsies were fixed in 4% paraformaldehyde, decalcified in 150 mM EDTA, washed in 70% ethanol and embedded in paraffin. Sections of 5-µm bone marrow biopsies were deparaffinized in xylene and rehydrated with a graded series of ethanol. Antigen retrieval was achieved by microwave treatment in EDTA (1 mM, pH 8.0). Endogenous peroxidase activity was quenched by incubating slides with Bloxall (Vector Laboratories), sections were blocked with avidin/biotin blocking solution (Vector Laboratories) for 15 min each, and Fc receptors were saturated with 5% normal human serum and 5% normal serum matching the host species of the secondary antibody in 10 mM Tris buffer, 5 mM EDTA, 0.15 M NaCl, 0.25% gelatin and 0.05% Tween-20 (pH 8.0).

For CD138/CD44/CXCL12 staining, tissue sections were incubated overnight at 4 °C with mouse anti–human CXCL12 (1:50; 79018, ThermoFisher) together with rat anti–human CD44 (1:50; IM7, ThermoFisher) in PBS containing 2% normal human serum. After incubation, the slides were washed thoroughly with PBS and incubated with AF647-conjugated donkey anti–mouse (1:100; Invitrogen) and horseradish peroxidase (HRP)-labeled goat anti–rat (1:250; Jackson ImmunoResearch) secondary antibodies supplemented with 2% normal human serum for 1 h at 20 °C. After rinsing in PBS and blocking free binding sites of the secondary antibody with 10% normal mouse serum, tissue sections were incubated with biotinylated CD138 (1:50; B-A38, Aviva) for 1 h at 20 °C followed by incubation with Avidin-AF488 (1:100; ThermoFisher) for 1 h at 20 °C in PBS containing 5% normal human serum. CD44 was developed in AF555 using Tyramide signal amplification (Invitrogen) according to the manufacturer's protocol.

For CD3/CD44/CXCL12 staining, sections were incubated overnight at 4 °C with mouse anti–human CXCL12 (1:50; 79018, ThermoFisher) together with rat anti–human CD44 (1:50; IM7, ThermoFisher) and rabbit anti–human CD3 (1:50; A0452, Dako) in PBS containing 2% normal human serum. After incubation, slides were washed thoroughly with PBS and incubated with AF647-conjugated donkey anti–rabbit (1:100; Invitroge), AF488-conjugated donkey anti–mouse (1:100; Invitrogen) and HRP-labeled goat anti–rat (1:250; Jackson ImmunoResearch) secondary antibodies supplemented with 2% normal human serum for 1 h at 20 °C.

CD44 was developed in AF555 using Tyramide signal amplification (Invitrogen) according to the manufacturer's protocol. Sections were mounted with ProLong Diamond containing DAPI (Invitrogen) and analyzed on a Leica DMRXA.

Statistical analyses. Statistical analysis was performed in R (version 3.6.1) or Graphpad Prism 8.2.1. All results in graphs are presented as means ± s.e.m. unless specified otherwise. Tests used to evaluate statistical significance are detailed in the figure legends.

Reporting Summary. Further information on research design is available in the Nature Research Reporting Summary linked to this article.

Data availability

The single-cell RNA sequencing datasets of the immune and non-hematopoietic bone marrow microenvironment and plasma cells of newly diagnosed individuals with MM and individuals without myeloma are available on ArrayExpress, no. E-MTAB-9139. The bulk RNA-sequencing datasets of the non-hematopoietic bone marrow microenvironment of individuals with MM at diagnosis and after induction treatment are available on ArrayExpress, no. E-MTAB-9285. Files summarizing receptor–ligand interactions as computed by CellphoneDB between the non-hematopoietic, CD38$^-$, CD38$^+$SDC1$^-$ and CD38$^+$SDC1$^+$ datasets are available through GitHub (https://github.com/MyelomaRotterdam/Microenvironment). Source data are provided with this paper.

Code availability

The code generated during this study to analyze the single-cell datasets is available through GitHub at https://github.com/MyelomaRotterdam/Microenvironment.

References

51. Satija, R., Farrell, J. A., Gennert, D., Schier, A. F. & Regev, A. Spatial reconstruction of single-cell gene expression data. *Nat. Biotechnol.* **33**, 495–502 (2015).
52. Stuart, T. et al. Comprehensive integration of single-cell data. *Cell* **177**, 1888–1902 (2019).
53. Waltman, L. & van Eck, N. J. A smart local moving algorithm for large-scale modularity-based community detection. *Eur. Phys. J. B* **86**, 471 (2013).
54. McInnes, L., Healy, J., Saul, N. & Grossberger, L. UMAP: uniform manifold approximation and projection. *J. Open Source Softw.* **3**, 861 (2018).
55. Mootha, V. K. et al. PGC-1α-responsive genes involved in oxidative phosphorylation are coordinately downregulated in human diabetes. *Nat. Genet.* **34**, 267–273 (2003).
56. Subramanian, A. et al. Gene set enrichment analysis: a knowledge-based approach for interpreting genome-wide expression profiles. *Proc. Natl Acad. Sci. USA* **102**, 15545–15550 (2005).
57. Cao, J. et al. The single-cell transcriptional landscape of mammalian organogenesis. *Nature* **566**, 496–502 (2019).
58. Patro, R., Duggal, G., Love, M. I., Irizarry, R. A. & Kingsford, C. Salmon provides fast and bias-aware quantification of transcript expression. *Nat. Methods* **14**, 417–419 (2017).
59. Soneson, C., Love, M. I. & Robinson, M. D. Differential analyses for RNA-seq: transcript-level estimates improve gene-level inferences. *F1000Res* **4**, 1521 (2015).
60. Love, M. I., Huber, W. & Anders, S. Moderated estimation of fold change and dispersion for RNA-seq data with DESeq2. *Genome Biol.* **15**, 550 (2014).
61. Stephens, M. False discovery rates: a new deal. *Biostatistics* **18**, 275–294 (2016).

Acknowledgements

We thank members of Myeloma Research Rotterdam and the Department of Hematology for critical discussions and reading of the manuscript, and the participants, families and nurses for their contributions to this study. We thank N. Leimkühler (Department of Hematology, Erasmus MC, the Netherlands) for help with the collection of healthy bone marrow biopsies and E. Bindels (Department of Hematology, Erasmus MC, the Netherlands) for help with sequencing. This work was supported by grants from the European Myeloma Network (EMN, grant HO95-EMN02-FB01102018 to P.S.) and ZonMw (grant 95103008 to P.S.). C.K. is supported by the Jose Carreras Leukaemia Foundation (grant DJCLS 17R/2018), the Deutsche Krebshilfe (grant 70112392), Deutsche Forschungsgemeinschaft (grant KH331/2–3) and the intramural funding of the faculty of Medicine at University Hospital of Muenster (grant Kha2/002/20). This project received funding from the European Union's Horizon 2020 research and innovation program under the Marie Skłodowska-Curie grant agreement no. 707404 (to Z.K.). The opinions expressed in this document reflect only the authors' views. The European Commission is not responsible for any use that may be made of the information it contains.

Author contributions

T.C. and P.S. conceptualized the study. T.C. and M.D.J. were responsible for the study methodology. M.D.J., Z.K., N.P. and S.T. were responsible for study investigation. M.D.J., Z.K., N.P., S.T., R.H., M.S. and T.C. analyzed the data. D.H.O.B., P.V.D.W, P.K.B., C.K., J.V., P.M., M.V.D. and A.B. provided resources for the study. M.D.J., R.H. and M.S. curated the data. M.D.J. contributed to data visualization. M.D.J. and T.C. wrote the original draft, and all authors reviewed and edited the final manuscript. P.S. and Z.K. acquired funding. T.C., A.B. and P.S. supervised the study, and T.C. and P.S. were responsible for project administration.

Competing interests

J.V. is an employee of Janssen; A.B. consults for Celgene, Janssen, Amgen and Takeda; P.S. consults for and receives research support from Celgene, Janssen, Karyopharm and SkylineDx; P.M. is on the advisory boards of and receives honoraria from Janssen, BMS/Celgene, Amgen and Abbvie. The remaining authors declare no competing interests.

Additional information

Extended data is available for this paper at https://doi.org/10.1038/s41590-021-00931-3.

Supplementary information The online version contains supplementary material available at https://doi.org/10.1038/s41590-021-00931-3.

Correspondence and requests for materials should be addressed to P.S. or T.C.

Peer review information *Nature Immunology* thanks Nicola Giuliani, Shannon Turley and the other, anonymous, reviewer(s) for their contribution to the peer review of this work. Peer reviewer reports are available. L. A. Dempsey was the primary editor on this article and managed its editorial process and peer review in collaboration with the rest of the editorial team.

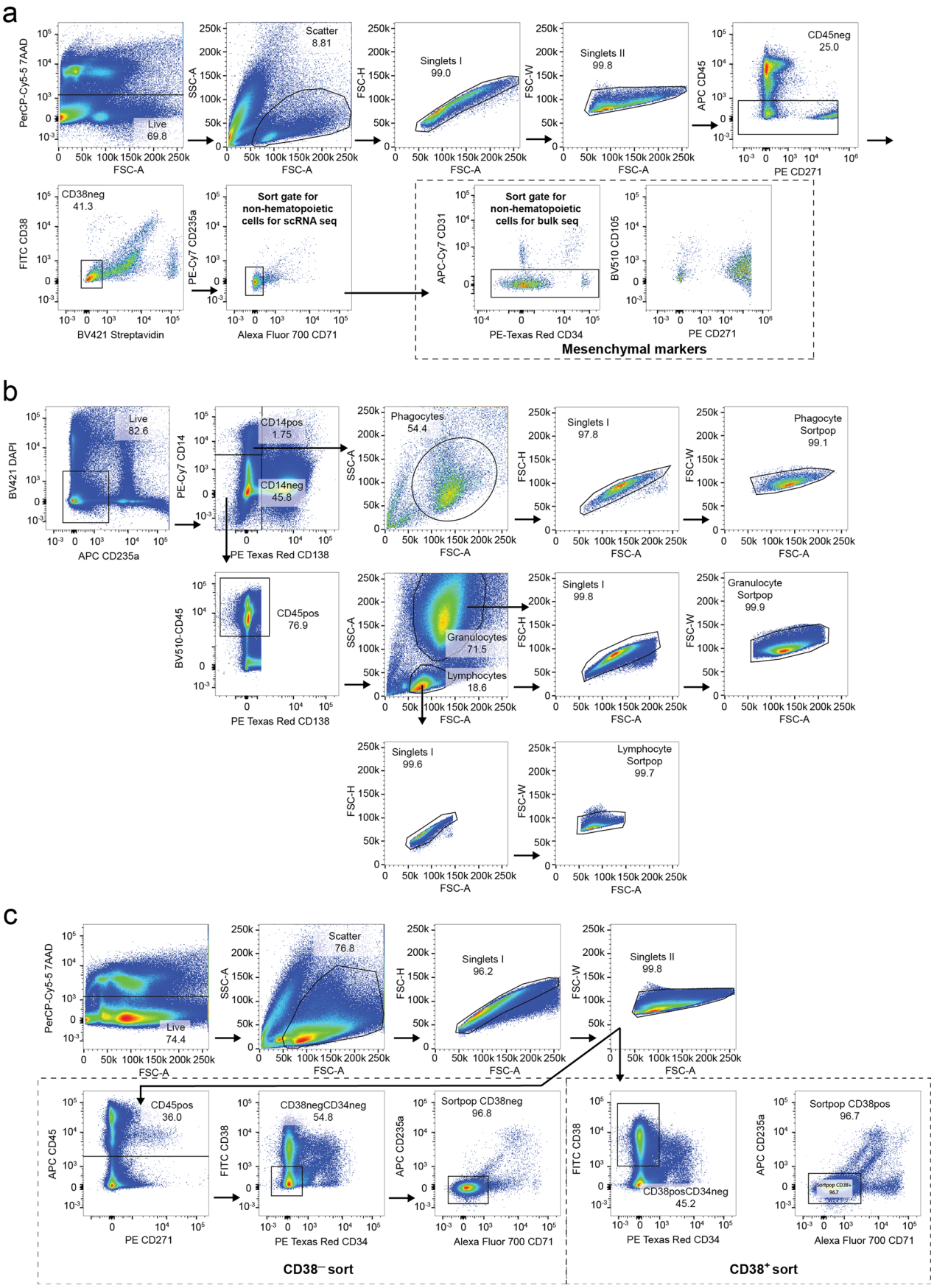

Extended Data Fig. 1 | See next page for caption.

Extended Data Fig. 1 | Related to Figs. 1, 4 and 6. (**a**) FACS gating strategy for total non-hematopoietic cells or bone marrow mesenchymal stromal cells from CD45-depleted bone marrow mononuclear cells (MNCs) from aspirates for bulk RNA sequencing and single-cell RNA sequencing experiments (**b**) FACS gating strategy of major immune cell populations in bone marrow aspirates for qPCR. (**c**) FACS gating strategy of $CD38^-$ and $CD38^+$ hematopoietic cells from non-depleted bone marrow aspirate MNCs for single-cell RNA sequencing experiments.

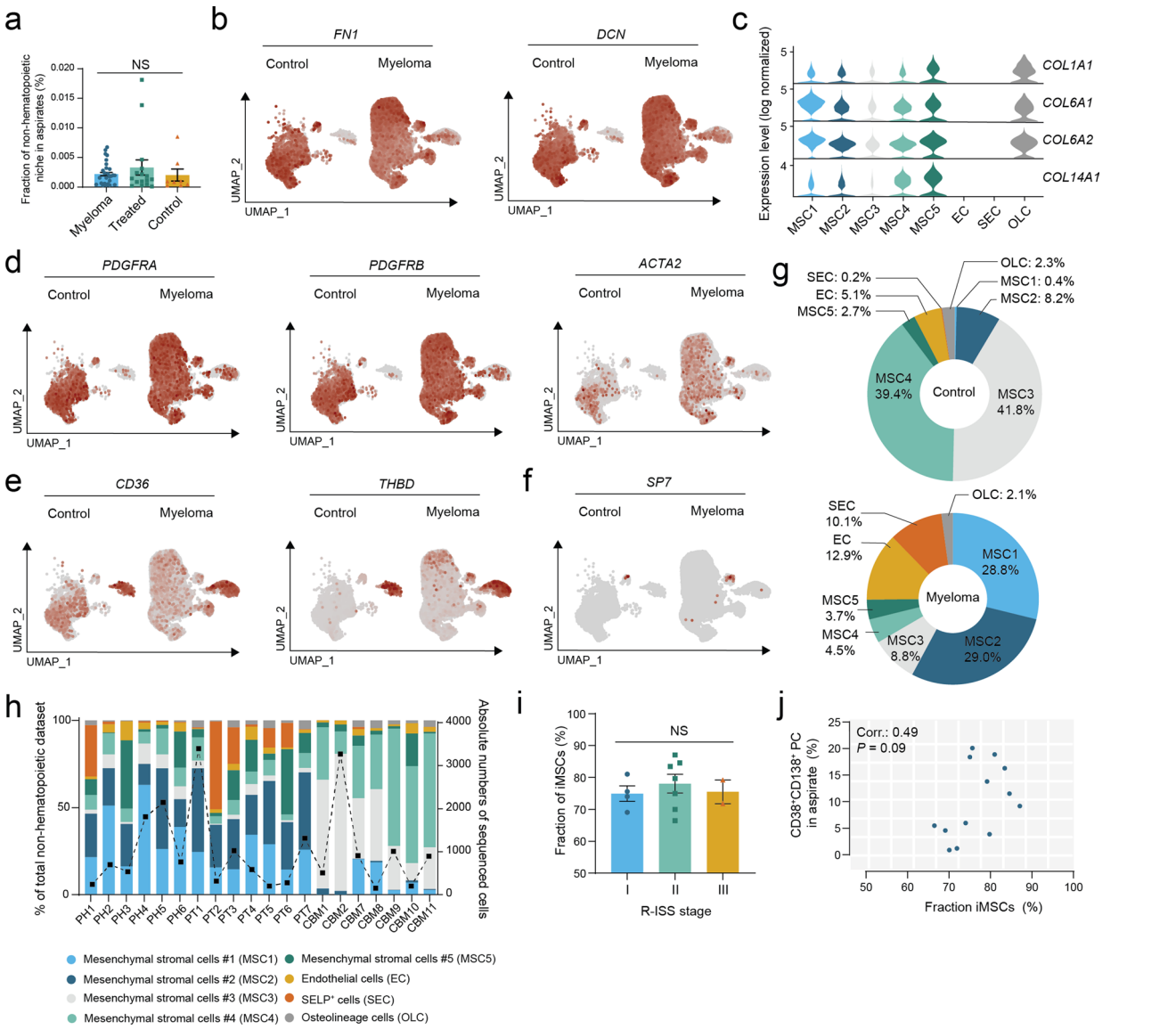

Extended Data Fig. 2 | See next page for caption.

Extended Data Fig. 2 | Related to Fig. 1. (**a**) Bar graph depicting relative abundance of non-hematopoietic cells of total bone marrow aspirates. Data points represent patients (myeloma, n = 40; treated, n = 16; control, n = 8) (**b**) Transcription of FN1 and DCN in non-hematopoietic cells (**c**) Violin plots depicting transcription of collagen genes in the 8 clusters of non-hematopoietic cells (**d**) Transcription of PDGFRA, PDGFRB and ACTA2 in non-hematopoietic cells (**e**) Transcription of CD36 and THBD in non-hematopoietic cells (**f**) Transcription of SP7 in non-hematopoietic cells (**g**) Circle diagrams depicting cluster fractions of total in control- and myeloma datasets (**h**) Bar plot depicting fraction of cells per cluster per patient (left Y-axis); line graph depicting total number of sequenced non-hematopoietic cells per patient (right Y-axis) (**i**) Bar graph depicting patient-specific iMSC-fraction of total mesenchymal stromal cells, segregated by R-ISS stage. Datapoints represent patients (R-ISS stage I, n = 4; II, n = 7; III, n = 2) (**j**) Spearman (two-tailed) correlation of iMSC-fraction of total mesenchymal stromal cells with percentage of $CD38^{+}CD138^{+}$ plasma cells in aspirates taken at diagnosis. Datapoints represent patients (**k**) Heatmap of top 50 differentially expressed genes up in MSC1/2 compared to MSC3/4/5 (left) or down in MSC1/2 compared to MSC3/4/5 (right) as described in Supplementary Table 5. The data in (**a**) and (**i**) are presented as mean ± standard error of the mean (SEM). Significance was calculated using Mann-Whitney U (two-tailed). NS; $p > 0.05$.

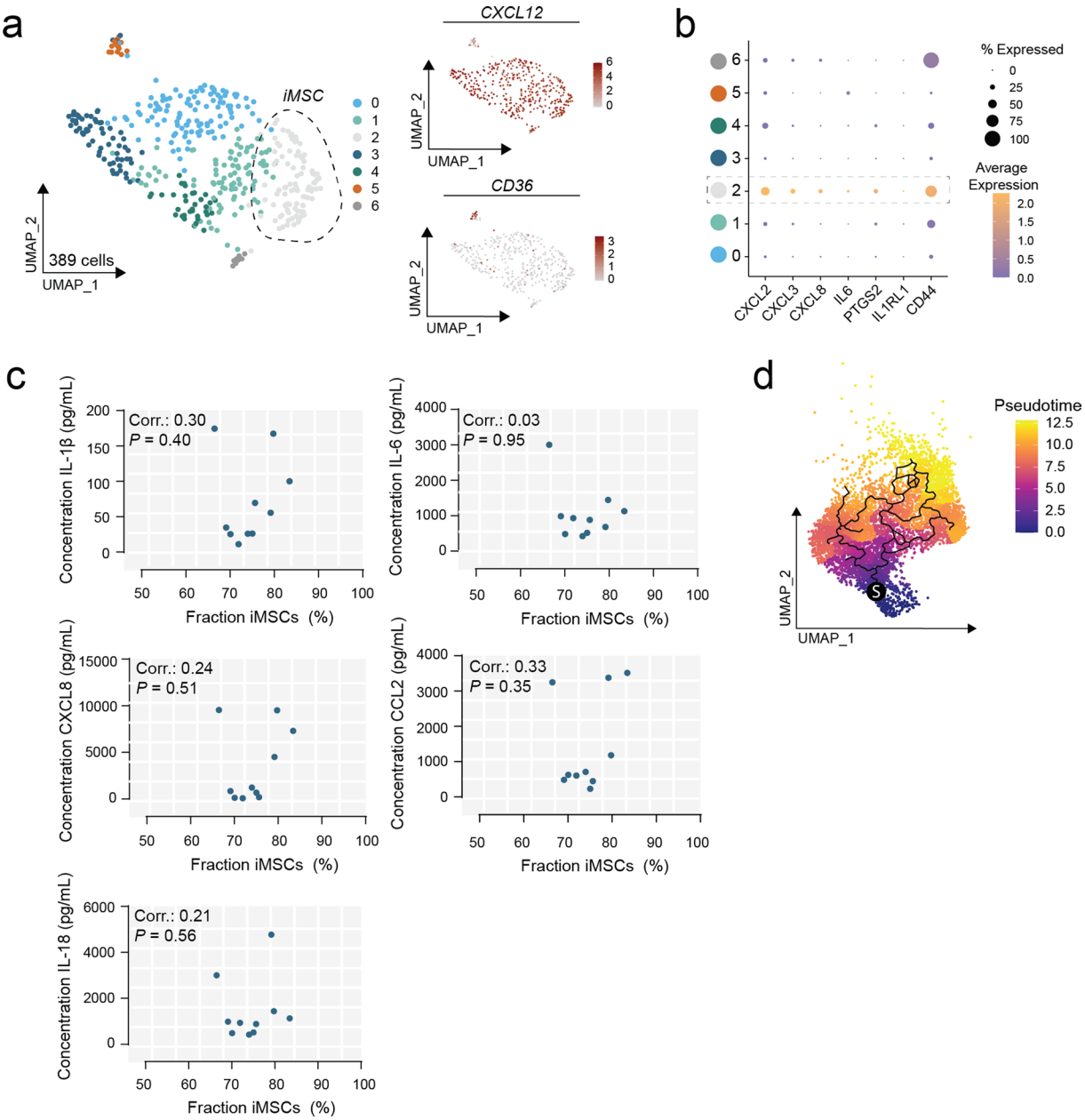

Extended Data Fig. 3 | Related to Figs. 1 and 3. (**a**) UMAP of the integrated dataset of 389 cells from freshly aspired bone marrow of 1 newly diagnosed myeloma patient showing 7 clusters identified by integrated analysis, accompanied by UMAPs showing transcription of CXCL12 (MSCs) and CD36 (endothelial cells). Colors represent clusters (**b**) Transcription of inflammatory genes in fresh non-hematopoietic cells shown in (**a**) (**c**) Spearman (two-tailed) correlation of iMSC-fraction of total mesenchymal stromal cells with inflammatory protein levels in bone marrow plasma. Datapoints represent patients (**d**) Monocle 3 pseudotime analysis of mesenchymal stromal cells in controls. 'S' represents arbitrary selected starting point of trajectory calculations.

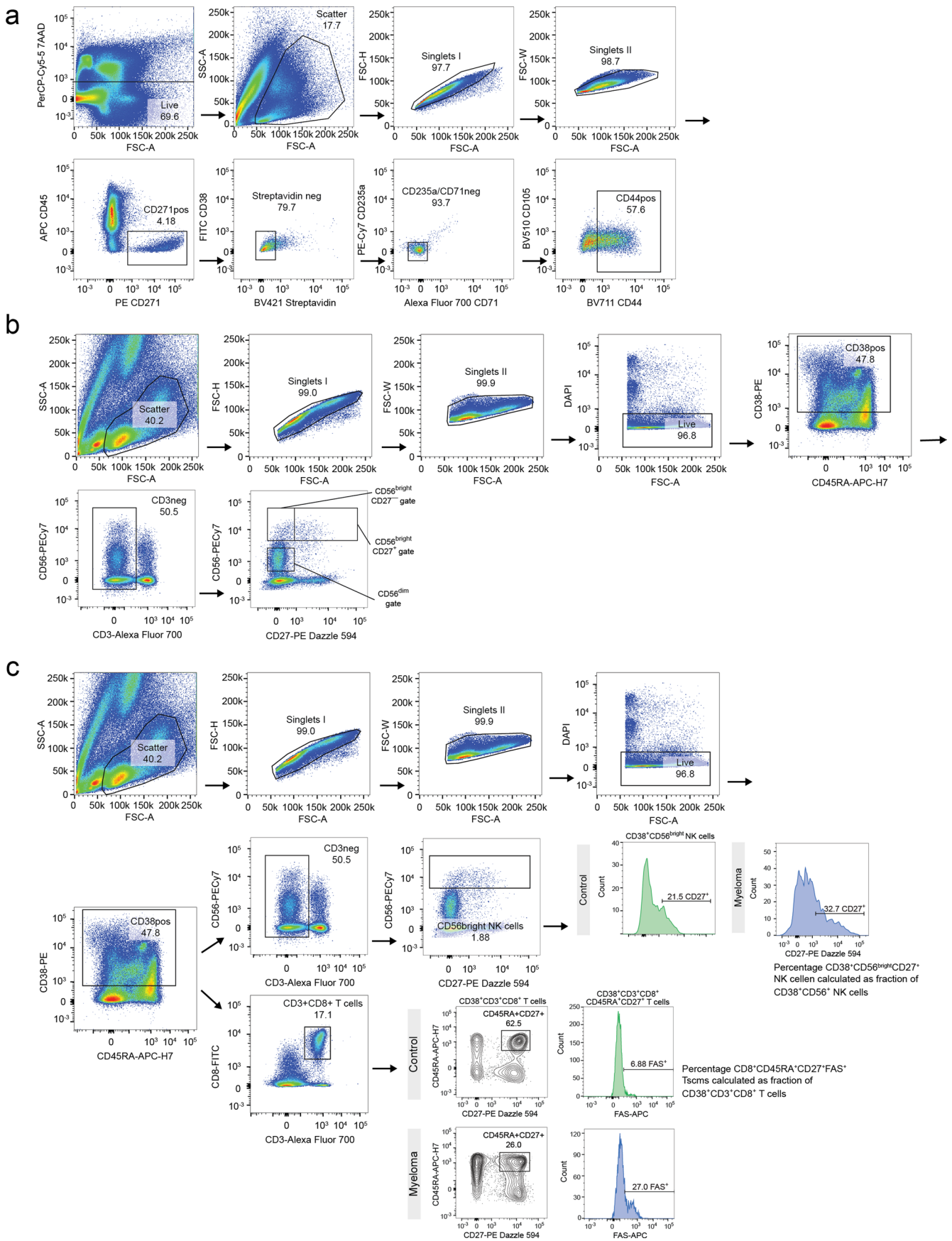

Extended Data Fig. 4 | See next page for caption.

Extended Data Fig. 4 | Related to Figs. 2 and 4. (**a**) Flow cytometric gating strategy to determine CD44 protein expression on $CD271^+$ MSCs (**b**) FACS gating strategy of $CD56^{dim}$, $CD56^{bright}$ and $CD56^{bright}CD27^+$ cells for qPCR (**c**) Flow cytometric gating strategy of $CD38^+CD3^+CD8^+CD45RA^+CD27^+FAS^+$ stem cell memory T cells, $CD38^+CD3^-CD56^{bright}$ NK cells and $CD38^+CD3^-CD56^{bright}CD27^+$ NK cells in bone marrow MNCs. Same sample as used for FACS in (**b**).

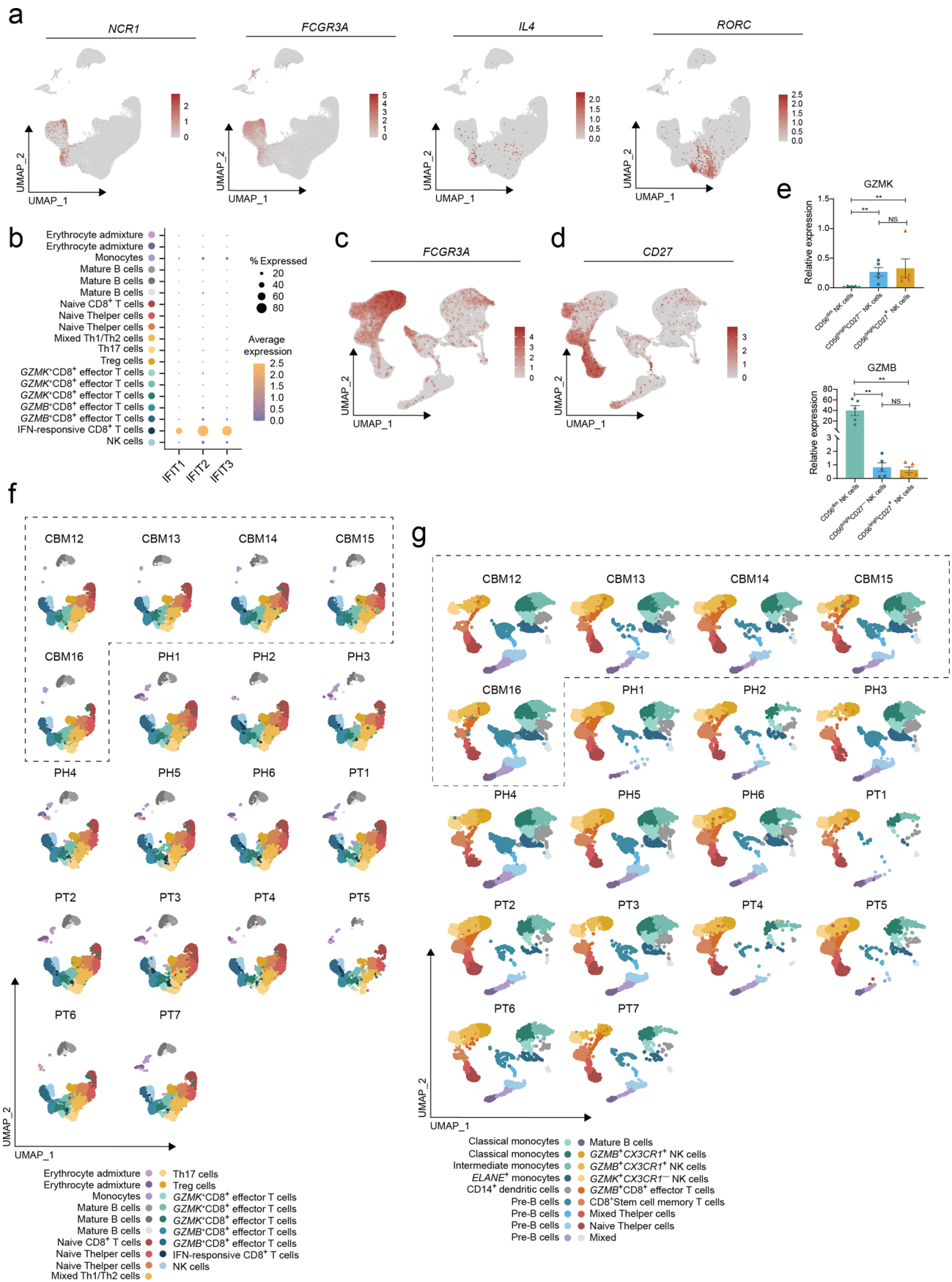

Extended Data Fig. 5 | See next page for caption.

Extended Data Fig. 5 | Related to Fig. 4. (**a**) Transcription of *NCR1*, *FCGR3A*, *IL4* and *RORC* in the CD38$^-$ dataset (**b**) Transcription of interferon-response genes *IFIT1*, *IFIT2* and *IFIT3* in the CD38$^-$ dataset (**c**) Transcription of *FCGR3A* in the CD38$^+$ dataset (**d**) Transcription of *CD27* in the CD38$^+$ dataset (**e**) Transcription of *GZMK* and *GZMB* in NK cell subsets of the myeloma bone marrow (n = 5) as determined by qPCR. Data are presented as mean ± standard error of the mean (SEM). Significance was calculated using Mann-Whitney U (two-tailed). **; $p \leq 0.01$ (**f**) Original UMAPs of CD38$^-$ dataset split by patient. CBM: non-myeloma control; PH: patient with hyperdiploid tumor; PT: patient with tumor harboring translocations (**g**) Original UMAPs of CD38$^+$ dataset split by patient. CBM: non-myeloma control; PH: patient with hyperdiploid tumor; PT: patient with tumor harboring translocations.

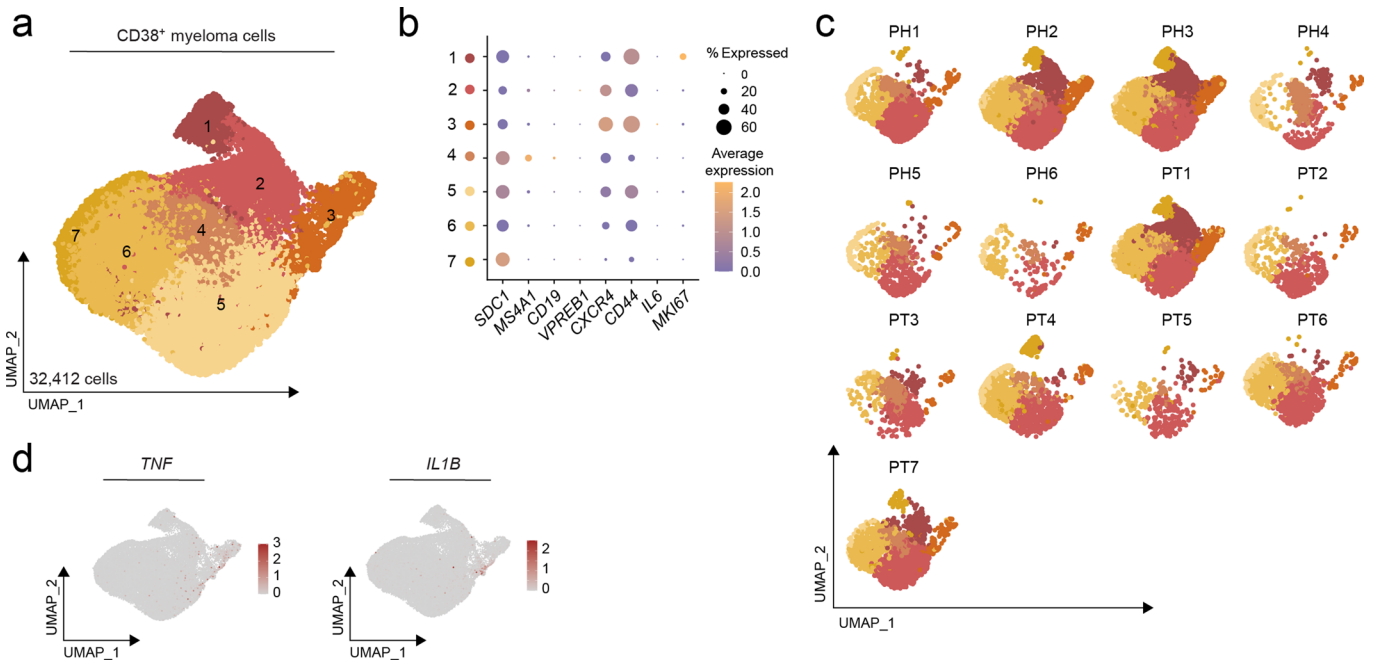

Extended Data Fig. 6 | Related to Fig. 4. (**a**) UMAP of 32,412 CD38$^+$SDC1$^+$ myeloma cells of 13 myeloma patients showing 7 clusters identified by integrated analysis. Colors represent clusters (**b**) Transcription of marker genes in the CD38$^+$SDC1$^+$ myeloma cell dataset (**c**) Original UMAPs of CD38$^+$SDC1$^+$ myeloma cell dataset split by patient. PH: patient with hyperdiploid tumor; PT: patient with tumor harboring translocations (**d**) Transcription of *TNF* and *IL1B* in the CD38$^+$SDC1$^+$ myeloma cell dataset.

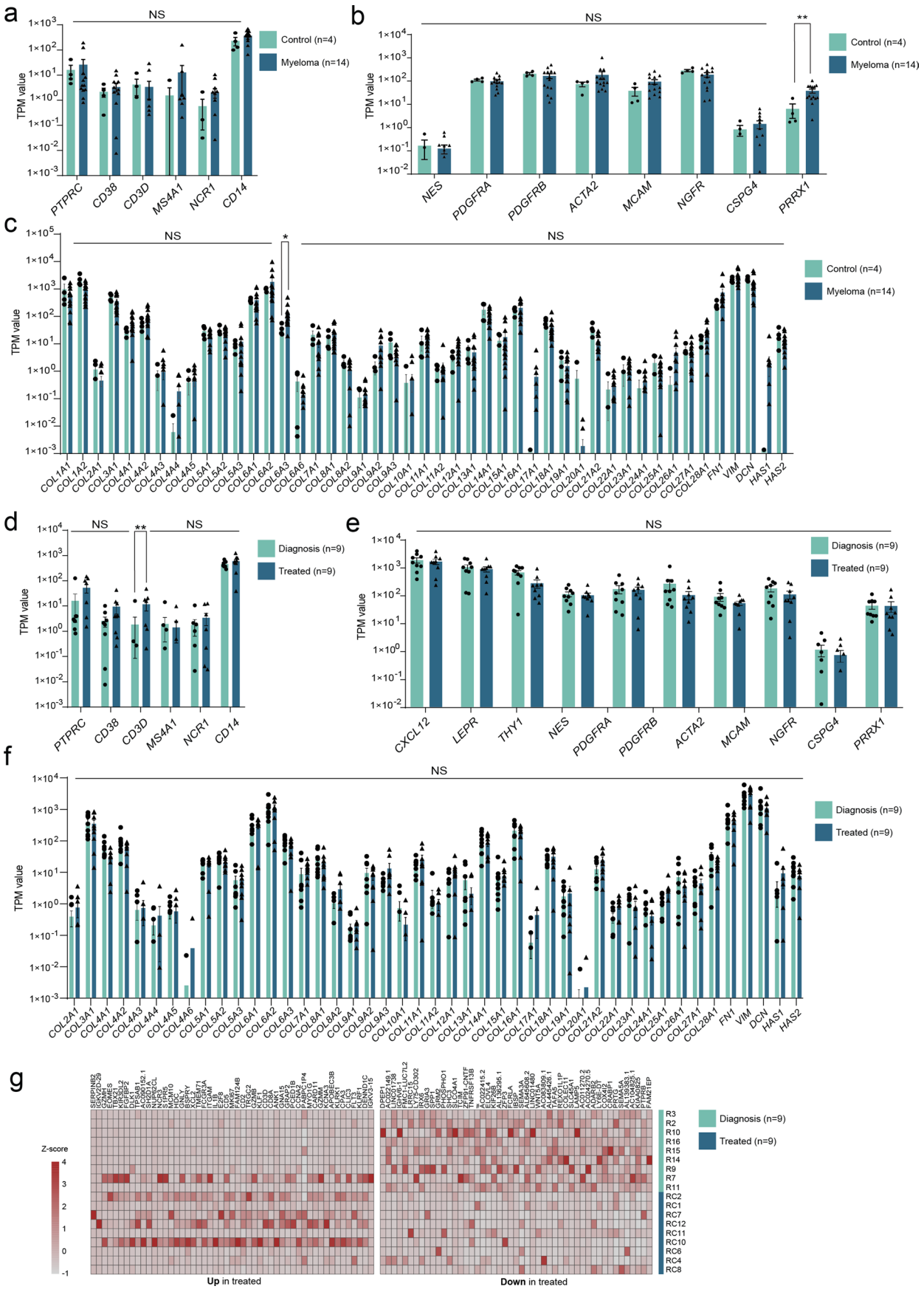

Extended Data Fig. 7 | See next page for caption.

Extended Data Fig. 7 | Related to Fig. 6. (**a**) Presence of canonical immune subset transcripts in bulk RNA sequencing datasets of purified MSC from newly-diagnosed myeloma (blue, n=14) and non-myeloma control patients (green, n=4) (**b**) Transcription of stromal cell subset markers comparing myeloma (blue) to non-myeloma (green) (**c**) Transcription of genes encoding extracellular matrix (ECM) proteins comparing myeloma (blue) to non-myeloma (green) (**d**) Transcription of canonical immune subset transcripts in bulk RNA sequencing datasets of purified MSC comparing post-induction treatment (blue, n = 9) to diagnosis (green, n = 9) (**e**) Transcription of stromal cell subset markers comparing post-induction treatment (blue) to diagnosis (green) (**f**) Transcription of genes encoding ECM proteins comparing post-induction treatment (blue) to diagnosis (green) (**g**) Heatmap of top differentially expressed genes up or down in treated patients compared to newly diagnosed samples as described in Supplementary Table 13. The data in (**a**), (**b**), (**c**), (**d**), (**e**) and (**f**) are presented as mean ± standard error of the mean (SEM). Significance was calculated using the Wald test (two-tailed), followed by Benjamini Hochberg correction. NS; $p > 0.05$, *; $p \leq 0.05$, **; $p \leq 0.01$. TPM; transcripts per million.

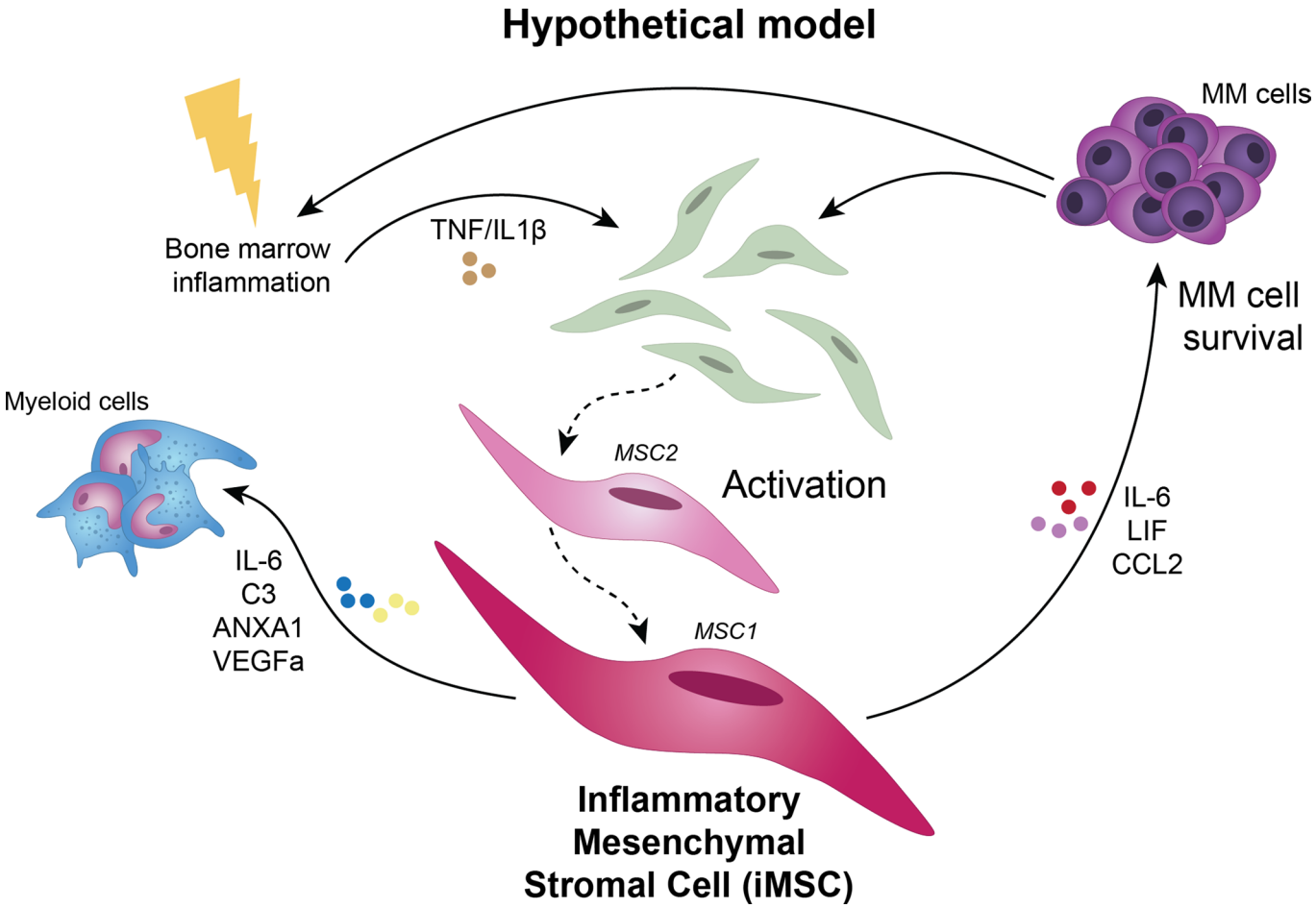

Extended Data Fig. 8 | Hypothetical model. Myeloma cells present in the bone marrow either activate stromal cells directly or trigger local inflammation, leading to the production of inflammatory mediators. Activation of local MSCs leads to formation of two subsets of iMSC (MSC2 and MSC1). iMSCs start to transcribe genes that might support MM cell survival and attract and modulate immune subsets, including myeloid cells.

nature research

Corresponding author(s): Tom Cupedo, Pieter Sonneveld

Last updated by author(s): 2021/04/01

Reporting Summary

Nature Research wishes to improve the reproducibility of the work that we publish. This form provides structure for consistency and transparency in reporting. For further information on Nature Research policies, see our Editorial Policies and the Editorial Policy Checklist.

Statistics

For all statistical analyses, confirm that the following items are present in the figure legend, table legend, main text, or Methods section.

n/a	Confirmed
☐	☒ The exact sample size (*n*) for each experimental group/condition, given as a discrete number and unit of measurement
☐	☒ A statement on whether measurements were taken from distinct samples or whether the same sample was measured repeatedly
☐	☒ The statistical test(s) used AND whether they are one- or two-sided *Only common tests should be described solely by name; describe more complex techniques in the Methods section.*
☐	☒ A description of all covariates tested
☐	☒ A description of any assumptions or corrections, such as tests of normality and adjustment for multiple comparisons
☐	☒ A full description of the statistical parameters including central tendency (e.g. means) or other basic estimates (e.g. regression coefficient) AND variation (e.g. standard deviation) or associated estimates of uncertainty (e.g. confidence intervals)
☐	☒ For null hypothesis testing, the test statistic (e.g. *F*, *t*, *r*) with confidence intervals, effect sizes, degrees of freedom and *P* value noted *Give P values as exact values whenever suitable.*
☐	☒ For Bayesian analysis, information on the choice of priors and Markov chain Monte Carlo settings
☒	☐ For hierarchical and complex designs, identification of the appropriate level for tests and full reporting of outcomes
☐	☒ Estimates of effect sizes (e.g. Cohen's *d*, Pearson's *r*), indicating how they were calculated

Our web collection on statistics for biologists contains articles on many of the points above.

Software and code

Policy information about availability of computer code

Data collection	BD FACSDiva v 5.0, Agilent 2100 Expert software v B.02.11.SI811, Leica Application Suite v 3.4, Applied Biosystems 7500 Fast Real-Time PCR System Software v 1.4.0.25, Perkin Elmer VICTOR X4 software v 4.0
Data analysis	Cellranger v 3.0.2 (10x Genomics), FlowJo v 10.6.1 (FlowJo LLC), R v 3.6.1, Seurat v 3.1.0 (Satija lab) and Seurat v 4.0.0 (Satija lab) which includes the used commands CellSelector and FindNeighbors (SNN modularity) as mentioned in the methods, Monocle 3 v 0.2.3. (Trapnell lab), CellphoneDB v 2.0 (Teich lab), fqtrim v 0.9.7 (http://ccb.jhu.edu/software/fqtrim/), Salmon v 1.2.1, tximport v 1.16 , DESeq2 v 1.28, GSEA software v 3.0 (Broad Institute), LegendPlex Data Analysis Software Suite v 2020.12.15 (BioLegend/Qognit), GraphPad Prism v 8.2.1 (Prism).

For manuscripts utilizing custom algorithms or software that are central to the research but not yet described in published literature, software must be made available to editors and reviewers. We strongly encourage code deposition in a community repository (e.g. GitHub). See the Nature Research guidelines for submitting code & software for further information.

Data

Policy information about availability of data

All manuscripts must include a data availability statement. This statement should provide the following information, where applicable:

- Accession codes, unique identifiers, or web links for publicly available datasets
- A list of figures that have associated raw data
- A description of any restrictions on data availability

See our data availability statement in the main documentation.

Field-specific reporting

Please select the one below that is the best fit for your research. If you are not sure, read the appropriate sections before making your selection.

☒ Life sciences ☐ Behavioural & social sciences ☐ Ecological, evolutionary & environmental sciences

For a reference copy of the document with all sections, see nature.com/documents/nr-reporting-summary-flat.pdf

Life sciences study design

All studies must disclose on these points even when the disclosure is negative.

Sample size	No sample-size calculation was performed. The identified differences between myeloma patients and controls are observed in all patients analyzed.
Data exclusions	Samples R8 and R13 were excluded from bulk sequencing analysis, since the sequenced libraries generated from these patients were contaminated with hematopoietic transcripts. We therefore concluded that these libraries did not consist of purified mesenchymal stromal cells. This is made clear in Supplemental Table 9.
Replication	Single cell sequencing experiment were non-repeated measurements of individual patients. Bulk sequencing experiments were non-repeated measurements individual patients. Flow cytometry to quantify CD44+ MSCs, stem cell memory T cells and GZMK+ NK cells were non-repeated measurements individual patients. All measurement were performed on seperate days. Immunohistochemistry of CD44+ iMSCs with CD138+ PCs included analysis of 20 individual myeloma patients and 5 individual controls divided over 4 experiments. Immunohistochemistry of CD44+ iMSCs with CD3+ PCs included analysis of 10 individual myeloma patients and 2 individual controls divided over 2 experiments. Stimulation cultures were individually performed per patient/control, including duplo's. qPCRs were carried out in 3 separate experiments.
Randomization	No randomization was performed. Samples were selected on cellularity of aspirate.
Blinding	Blinding was not relevant since the goal of the study was to identify all differences between myeloma and controls.

Reporting for specific materials, systems and methods

We require information from authors about some types of materials, experimental systems and methods used in many studies. Here, indicate whether each material, system or method listed is relevant to your study. If you are not sure if a list item applies to your research, read the appropriate section before selecting a response.

Materials & experimental systems

n/a	Involved in the study
☐	☒ Antibodies
☒	☐ Eukaryotic cell lines
☒	☐ Palaeontology and archaeology
☒	☐ Animals and other organisms
☐	☒ Human research participants
☐	☒ Clinical data
☒	☐ Dual use research of concern

Methods

n/a	Involved in the study
☒	☐ ChIP-seq
☐	☒ Flow cytometry
☒	☐ MRI-based neuroimaging

Antibodies

Antibodies used

For depletion: biotinylated anti-CD45 (HI30, BioLegend, cat. 304004), anti-CD235a (HIR2, BioLegend, cat. 306618) and anti-CD38 (from human CD38 MicroBead Kit, Miltenyi Biotec, cat. 130-092-263)

For flow cytometry CD271-PE (ME20.4, BioLegend, cat. 345106), CD235a-PECy7 (HI264, BioLegend, cat. 349112), CD31-APCCy7 (WM59, BioLegend, cat. 303120), CD44-BV711 (IM7, BioLegend, 103057), streptavidin-BV421 (BioLegend, cat. 405225), CD34-PECF610 (4H11, eBioscience, cat. 61-0349-42), CD45-APC (2D1, eBioscience, cat. 17-9459-42), CD38-FITC (MHCD3801, Life Technologies, cat. MHCD3801), CD71-Alexa Fluor 700 (MEM-75, ExBio, cat. A7-235-T100), CD105-BV510 (266, BD Biosciences, cat. 563264), CD45-BV510 (HI30, Sony, cat. 2120175), CD14-PECy7 (HCD14, BioLegend, cat. 325617), CD138-PECF594 (MI15, BD Biosciences, cat. 564606), CD235a-APC (GA-R2, BD Biosciences, cat. 551336), CD95-APC (DX2, BD Pharmingen, cat. 558814), CD45RA-APC-H7 (HI100, BD Pharmingen, cat. 560674), CD3-Alexa Fluor 700 (UCHT1, BD Pharmingen, cat. 557943), CD122-PerCP-Cy5.5 (TU27, BioLegend, cat. 339011), CD27-PE Dazzle 594 (M-T271, BioLegend, cat. 356421), CD56-PECy7 (CMSSB, eBioscience, 25-0567-42), CD38-PE (HB-7, BD Biosciences, cat. 345806) and CD8-FITC (MEM-31, ImmunoTools, cat. 21270083).

For immunohistochemistry: biotinylated mouse anti-human CD138 (B-A38, Aviva Systems Biology, cat. OADB00060), mouse anti-

human CXCL12 (79018, ThermoFisher, cat. MA5-23759), rat anti-human CD44 (IM7, ThermoFisher, cat. 14-0441-85), rabbit anti-human CD3 (polyclonal, DAKO, A0452), donkey anti-mouse AF647 (ThermoFisher, A32787), donkey anti-rabbit AF647 (ThermoFisher, A31573), goat anti-rat HRP (Jackson ImmunoResearch, cat 112-035-003), avidin-AF488 (ThermoFisher, cat S11223).

Validation

All reagents are from commercial vendors as outlined above. Specificity was based on descriptions provided by the manufacturers, the data sheets and previously published clones and fluorochromes. Antibodies were titrated on relevant cells or tissues prior to use. Validation of secondary antibody from Jackson immunoresearch was performed by staining of slides in the absence of primary antibody.

Vendor-specific information:
All antibodies from Biolegend were quality control tested by immunofluorescent staining with flow cytometric analysis. (www.biolegend.com/en-us/reproducibility)
All antibodies from Invitrogen/eBioscience were tested for target specificity and for use in flow cytometry (https://www.thermofisher.com/nl/en/home/life-science/antibodies/invitrogen-antibody-validation.html)
For BD Biosystems all antibodies are quality control (QC) tested in primary model systems to ensure biological accuracy in an ISO 9001 certified facility.
For Immunotools antibodies the vendor validation procedure is unknown.
All Aviva Biosystems antobodies are evaluated using either cell lines or tissue samples with standard assays such as ECL based Western Blotting, Immunohistochemistry (ICH), and immunoprecipitation (IP). (https://www.avivasysbio.com/technical-resources)
The Dako polyclonal antibody specificity was validated in western blot and immunoprecipitation.

Human research participants

Policy information about studies involving human research participants

Population characteristics

The study uses retrospective analyses of patient samples collected in the context of the Cassiopeia clinical trial (ClinicalTrials.gov Identifier: NCT02541383)

Participants in the Cassiopeia trial were ages 18-65 years, all sexes are eligible for study.

Inclusion criteria were: diagnosis of previously untreated multiple myeloma (MM); have a confirmed diagnosis and eligible for high dose chemotherapy and autologous stem cell transplantation, and an Eastern Cooperative Oncology Group (ECOG) performance status score of 0,1 or 2

Exclusion criteria were: previous treatment for Multiple Myeloma; Primary amyloidosis, plasma cell leukemia or smoldering Multiple Myeloma; prior or concurrent exposure to systemic therapy or SCT (Stem Cell Transplantation) for any plasma cell dyscrasia, with the exception of an emergency use of a short course (equivalent of dexamethasone 40 mg/day for a maximum 4 days) of corticosteroids before treatment, or received an investigational drug or used an invasive investigational medical device within 4 weeks before Cycle 1, Day 1; history of malignancy (other than Multiple Myeloma) within 10 years before the date of randomization, except for the following if treated and not active: basal cell or nonmetastatic squamous cell carcinoma of the skin, cervical carcinoma in situ, ductal carcinoma in situ of breast, or International Federation of Gynecology and Obstetrics (FIGO) Stage 1 carcinoma of the cervix; known chronic obstructive pulmonary disease (COPD) or moderate to severe asthma; any concurrent medical or psychiatric condition or disease (eg, autoimmune disease, active systemic disease, myelodysplasia) that is likely to interfere with the study procedures or results, or that in the opinion of the investigator, would constitute a hazard for participating in this study.

Recruitment

Patients were previously recruited in the context of the Cassiopeia clinical trial, an international multicenter trial.
Selection of patient samples to be used in the research published here was based on number of cells in aspirate, since MSCs in bone marrow aspirates are a rare population. This not withstanding, as can be observed in Extended Data table 2, selection for cell-rich samples was not associated with higher numbers of tumor load and likely represents sampling variation during aspiration.

Ethics oversight

Medical ethical commitees of the ErasmusMC Rotterdam and of the Univerity hospital Munster

Note that full information on the approval of the study protocol must also be provided in the manuscript.

Clinical data

Policy information about clinical studies

All manuscripts should comply with the ICMJE guidelines for publication of clinical research and a completed CONSORT checklist must be included with all submissions.

Clinical trial registration

NCT02541383

Study protocol

The full study protocol can be accessed on ClinicalTrials.gov Identifier: NCT02541383, or at https://hovon.nl/en/trials/ho131

Data collection

The data described in this study were collected at the ErasmusMC in Rotterdam, using cells from patients enrolled in the Cassiopeia trial. The experiments described in our study are independent from the clinical trial objectives and independent of treatment arms. With the exception of the bulk sequencing on 9 patients in figure 6, all samples used were from untreated newly diagnosed patients.

Outcomes

Primary and secondary outcomes are published in Moreau P et al. 'Bortezomib, thalidomide, and dexamethasone with or without daratumumab before and after autologous stem-cell transplantation for newly diagnosed multiple myeloma (CASSIOPEIA): a

randomised, open-label, phase 3 study'. Lancet. 2019 Jul 6;394(10192):29-38. doi: 10.1016/S0140-6736(19)31240-1. Epub 2019 Jun 3. Erratum in: Lancet. 2019 Jun 14;: PMID: 31171419.

Flow Cytometry

Plots

Confirm that:

☒ The axis labels state the marker and fluorochrome used (e.g. CD4-FITC).

☒ The axis scales are clearly visible. Include numbers along axes only for bottom left plot of group (a 'group' is an analysis of identical markers).

☒ All plots are contour plots with outliers or pseudocolor plots.

☒ A numerical value for number of cells or percentage (with statistics) is provided.

Methodology

Sample preparation	Work-up prior to scRNA sequencing and bulk sequencing: Viably frozen bone marrow aspirates were thawed in DMEM + 10% FCS according to the 10X Genomics protocol 'Fresh Frozen Human Peripheral Blood Mononuclear Cells for Single Cell RNA sequencing'. Only samples containing >200x106 MNCs were included. Fc receptors were blocked in 10% normal human AB serum (Sigma-Aldrich). For enrichment of stromal mesenchymal cells, samples were incubated with biotinylated antibodies against CD45 (clone HI30, BioLegend), CD235a (clone HIR2, BioLegend) and CD38 (from human CD38 MicroBead Kit, Miltenyi Biotec) followed by depletion using magnetic anti-biotin beads (Miltenyi Biotec) and the iMag (BD Biosciences). After depletion, cells were stained for sorting in PBS containing 2% FCS at 4°C. After staining, cells were washed and resuspended in PBS containing 2% FCS + 7AAD or DAPI. Work-up prior to flow cytometric analyses: Viably frozen bone marrow aspirates were thawed in DMEM + 10% FCS according to the 10X Genomics protocol 'Fresh Frozen Human Peripheral Blood Mononuclear Cells for Single Cell RNA sequencing'. Fc receptors were blocked in 10% normal human AB serum (Sigma-Aldrich). Then, cells were stained for analysis in PBS containing 2% FCS at 4°C. After staining, cells were washed and resuspended in PBS containing 2% FCS + DAPI. Cytokine/Chemokine analyses: Bone marrow supernatant was collected from bone marrow aspirates after ficoll separation and stored at -80° until use. Prior to analyses, supernatant vials were spun down twice at 21,000 x g for 5 min, to pellet and discard lipid contents, debris and residual cells. Cytokine/chemokine concentrations were determined using LegendPlex human inflammation panel 1 (BioLegend) according to the manufacturer's recommendations.
Instrument	FACSAria III (BD Biosciences) and LSR II (BD Biosciences)
Software	BD FACSDiva v 5.0, FlowJo v 10.7.1 (FlowJo LLC)
Cell population abundance	Single cell sequencing of sorted mesenchymal and immune cells showed no admixture of other cell populations.
Gating strategy	Gating strategy is provided in the Supplementary Information. Preliminary FSC and SSC scatter gates were defined by FSC > 50.000. Boundaries between positive and negative staining cell populations were in most cases evident by several logs of seperation. If not, isotype controls were used. For isolation of non-hematopoietic cells, cells were gated on live cells (7AAD negative), followed by gating of relevant FSC/SSC populations and doublet exclusion. Next, there was subsequent gating of: CD45neg cells, CD38neg cells, streptavidin neg cells, CD235a neg cells and CD71neg cells. The negatively selected live cells were sorted for bulk sequencing and single cell RNA sequencing experiments. For hematopoietic cells for single cell RNA sequencing experiments, cells were gated on live cells (7AAD negative), followed by gating of relevant FSC/SSC populations and doublet exclusion. For the CD38- population, we selected CD45int and CD45pos cells, followed by CD38 and CD34 exclusion. Finally, CD235a and CD71 pos cells were excluded. The remaining population was sorted as CD38- hematopoietic cells. For the CD38+ population, we selected CD38int and CD38pos cells that were CD34neg. CD235a and CD71 pos cells were excluded, and the remaining population was sorted as CD38+ hematopoietic cells. For qPCR of TNF and IL1b in lymphocytes, granulocytes and monocytes, we first selected live DAPIneg and CD235a neg cells. Then we excluded CD138+ cells. Three populations were then selected: - We selected for CD14+ cells, selected the expected monocytic cells on FSC/SSC scatter and performed doublet exclusion. These cells were sorted as 'myeloid'. - We selected CD45int and CD45pos cells, selected the expected granulocytic cells on the FSC/SSC scatter and performed doublet exclusion. These cells were sorted as 'granulocytes'. - We selected CD45int and CD45pos cells, selected the expected lymphocytic cells on the FSC/SSC scatter and performed doublet exclusion. These cells were sorted as 'lymphocytes'. For quantification of CD44+ iMSCs, cells were gated on live cells (7AAD negative), followed by gating of relevant FSC/SSC populations and doublet exclusion. Next, there was subsequent gating of: CD271pos cells, CD38neg cells, streptavidin neg cells, CD235a neg cells and CD71neg cells. On the remaining population, the CD44+ gate was set using an isotype control.

For qPCR of GZMK and GZMB in NK cells, we selected expected location of the FSC/SSC scatter, followed by doublet exclusion. Then DAPIneg cells were selected, followed by selection of CD38+ cells. Then, CD3+ cells were excluded. Finally, three populations were selected using a CD56 versus CD27 plot:
- CD56brightCD27- NK cells
- CD56bright CD27+ NK cells
- CD56int NK cells

For quantification of CD56bright NK cells and stem cell memory T cells, we selected expected location of the FSC/SSC scatter, followed by doublet exclusion. Then DAPIneg cells were selected, followed by selection of CD38+ cells. The two populations were selected as follows:
- CD56bright NK cells were selected by first excluding CD3+ cells. Then, in a CD56 versus CD27 plot, we selected for CD56bright NK cells.
- Stem cell memory T cells were selected by first selecting CD3+CD8+ T cells. The resulting population was subsequently selected for CD45RA and CD27 double positive cells. Finally, we quantified FAS expression within the final population. The gate was set using an isotype control.

☒ Tick this box to confirm that a figure exemplifying the gating strategy is provided in the Supplementary Information.